

Optical/UV Emission in the Tidal Disruption Event ASASSN-14li: Implications of Disc Modeling

Sixiang Wen,^{1,2*} Peter G. Jonker,^{1,3} Nicholas C. Stone,⁴ Sjoert Van Velzen,⁵ and Ann I. Zabludoff,²

¹Department of Astrophysics/IMAPP, Radboud University, P.O. Box 9010, 6500 GL Nijmegen, The Netherlands

²University of Arizona, 933 N. Cherry Ave., Tucson, AZ 85721

³SRON, Netherlands Institute for Space Research, Niels Bohrweg 4, 2333 CA, Leiden, The Netherlands

⁴Racah Institute of Physics, The Hebrew University, Jerusalem, 91904, Israel

⁵Leiden Observatory, Leiden University, Postbus 9513, 2300 RA, Leiden, The Netherlands

Accepted 2023 March 30. Received 2023 February 18; in original form 2022 October 24

ABSTRACT

We predict late-time optical/UV emission from tidal disruption events (TDEs) from our slim accretion disc model (Wen et al. 2020) and explore the impact of the black hole mass M_{\bullet} , black hole spin a_{\bullet} , and accretion disc size. We use these synthetic spectra to successfully fit the multi-band *Swift* observations of ASASSN-14li at >350 days, setting only the host galaxy extinction and outer disc radius as free parameters and employing the M_{\bullet} , a_{\bullet} , disc inclination, and disc accretion rates derived from fitting 10 epochs of ASASSN-14li’s X-ray spectra with the slim disc. To address the nature of the early-time optical/UV emission, we consider two models: shock dissipation and reprocessing. We find that (1) the predicted late-time optical/UV colour (e.g., $u - w2$) is insensitive to black hole and disc parameters unless the disc spreads quickly; (2) a starburst galaxy extinction model is required to fit the data, consistent with ASASSN-14li’s post-starburst host; (3) surprisingly, the outer disc radius is $\approx 2\times$ the tidal radius and \sim constant at late times, showing that viscous spreading is slow or non-existent; (4) the shock model can be self-consistent if $M_{\bullet} \lesssim 10^{6.75} M_{\odot}$, i.e., on the low end of ASASSN-14li’s M_{\bullet} range ($10^{6.5-7.1} M_{\odot}$; 1σ CL); larger black hole masses require disruption of an unrealistically massive progenitor star; (5) the gas mass needed for reprocessing, whether by a quasi-static or an outflowing layer, can be $< 0.5 M_{\odot}$, consistent with a (plausible) disruption of a solar-mass star.

Key words: transients: tidal disruption events; accretion, accretion discs; black hole physics; (galaxies:) quasars: supermassive black holes

1 INTRODUCTION

Tidal disruption events (TDEs) happen when a star approaches a supermassive black hole (SMBH; (Hills 1975; Rees 1988)). After the star is broken down by tidal forces, half of the debris remains bound and can be accreted by the SMBH, producing a strong electromagnetic flare. These flares frequently emit at optical (van Velzen, et al. 2011; Gezari et al. 2012; Arcavi et al. 2014; Holoien et al. 2016; van Velzen et al. 2021), near-ultraviolet (NUV; Gezari et al 2006; Gezari et al. 2008), and soft X-ray (Bade et al. 1996; Greiner et al. 2000; Komossa et al. 2004; Saxton et al. 2021) wavelengths.

The source of TDE optical/UV emission is still a matter of debate. There are two leading models for the early (power-law decaying) optical/UV light: one is emission from a reprocessing layer, which is powered by the X-rays and extreme UV emanating from the inner accretion disc (Loeb & Ulmer 1997; Guillochon et al. 2014; Metzger & Stone 2016; Roth et al. 2016; Roth & Kasen 2018; Dai et al. 2018; Lu & Bonnerot 2019), and the other is shock-powered emission, often assumed to involve an outer shock that forms at the intersection of the debris streams near their orbital apocenters (Shiokawa et al. 2015; Piran et al. 2015), but sometimes also involving shocks between tidal debris and a circularizing accretion flow (Bonnerot &

Lu 2020; Steinberg & Stone 2022). Based on these two different paradigms, two modeling suites, MOSFiT (Mockler et al. 2019) and TDEMAsS (Ryu et al. 2020), respectively, have been used to constrain the masses of the SMBH and disrupted star by fitting the early observed optical/UV light curves. Both models yield SMBH mass constraints consistent with determinations from the black hole (BH) mass versus galaxy velocity dispersion relation (Ferrarese & Ford 2005; Kormendy & Ho 2013; McConnell & Ma 2013).

In contrast to the optical/UV emission, there is more consensus on the origin of TDE thermal X-rays, which are widely thought to be powered by accretion and to arise from an inner disc (Ulmer 1999). The X-ray spectra of the TDEs ASASSN-14li, ASASSN-15oi, and J2150 (Wen et al. 2020, 2021, hereafter W20 and W21) are consistent with those predicted by a general relativistic slim accretion disc model (Abramowicz et al. 1988); additional X-ray-producing mechanisms are not obviously required, although at late times often the mass accretion rate can be well below the Eddington limit (the disc may experience a hard state change, e.g., (Jonker et al. 2020)). From the X-ray spectral fitting of two TDEs, W20 found that the absorption parameter (i.e. the column density N_{H}), declines to the level predicted for the host galaxy plus Milky Way contribution after several hundred days. This behavior supports a picture in which,

* E-mail: S.Wen@astro.ru.nl

at late times, a gaseous reprocessing layer¹ becomes increasingly optically thin, and the optical/UV emission, which has dimmed by $\geq 10\times$, is dominated by a disc component (van Velzen, et al. 2019). It is therefore important to test whether the observed optical/UV emission at late times can be successfully fit with a bare slim disc model, after allowing for host dust extinction and (potentially) a time-varying outer disc radius.

In this paper, we focus on ASASSN-14li’s optical/UV emission, based on our successful fitting of its evolving X-ray spectrum (W20). ASASSN-14li was first discovered on 22 November 2014, in a post-starburst galaxy at $z = 0.0206$ (Jose et al. 2014). The optical/UV light curves initially declined quickly and then evolved more gradually after about 350 days (Brown et al. 2017). The slow late-time decay is consistent with disc-dominated emission (van Velzen, et al. 2019) and can be well fit by a time-dependent model of a viscously spreading, general relativistic thin disc (Mummery & Balbus 2020, hereafter MB20). In MB20, the accretion rate at each observing epoch is determined by the time-dependent disc equations, and the SMBH mass is constrained to $1.45 \times 10^6 < M_{\bullet}/M_{\odot} < 2.05 \times 10^6$ with a broad range of permitted BH spins.

The MB20 constraints on M_{\bullet} and spin are only marginally consistent (at the 2σ confidence level (CL)) with the slim disc fitting results of W20. In this paper, we perform a detailed study of the late optical/UV emission of ASASSN-14li based on the results obtained through fitting the X-ray spectra with the slim disc. Unlike the MB20 model, the disc accretion rate here is a free parameter and is determined by the X-ray spectral fits. We check whether (1) the slim disc solution can match the late time optical/UV light curves; (2) dust extinction in the host galaxy is important for the observed optical/UV emission; and (3) the size of the accretion disc evolves, i.e., whether angular momentum transport may cause the disc to spread out with time.

In addition to our modeling of the late-time light curves, we test two possible sources—a reprocessing debris layer or a shock arising from a self-intersecting debris stream—for the *early-time* optical/UV emission of ASASSN-14li. In these tests, we calculate the minimum mass of the disrupted star that can produce the observed optical/UV emission, where the inferred disc luminosity, M_{\bullet} , and dimensionless spin parameter a_{\bullet} are derived from the X-ray spectral fits.

The paper is organized as follows. We explore the general dependence of theoretical optical/UV light curves on M_{\bullet} , a_{\bullet} , and outer disc radius R_{out} in Section 2. We describe the (archival) optical/UV emission data for ASASSN-14li and our reduction procedure in Section 3. In Section 4, we show the fit results of the slim disc model to the observed late-time optical/UV light curves. In Section 5, we describe our tests of whether reprocessing or the shock paradigm can explain the bright early optical/UV emission. Finally, we summarize our conclusions in 6.

2 THEORETICAL OPTICAL/UV LIGHT CURVES

In this section, we calculate the late-time optical/UV emission from the slim disc model of W21. We use a multi-colour black body model to calculate the local optical/UV emission and a ray-tracing code (Psaltis & Johannsen 2011), which includes gravitational redshift, Doppler, and lensing effects self-consistently, to determine the

monochromatic flux. As the disc formed after a TDE is finite, the disc size becomes an important factor to the optical/UV emission. Here, we limit the disc to radii $R < R_{\text{out}}$, neglecting the small difference between our hard cutoff and the exponential cutoff used by MB20.

We explore the impact of M_{\bullet} , a_{\bullet} , and R_{out} on theoretical optical/UV light curves in Figure 1. In this analysis, we estimate the disc accretion rate from hydrodynamic simulations of the disruption process (Guillochon & Ramirez-Ruiz 2013), which can be determined from the time after peak, M_{\bullet} , the penetration parameter β , the progenitor star mass M_{\star} , and polytropic index (here we consider the case of $\gamma = 4/3$). The left plot shows the light curves for different values of M_{\bullet} and a_{\bullet} ; we fix the disc outer radius to $R_{\text{out}} = 2R_t/\beta$ (R_t is tidal radius). A larger M_{\bullet} always results in a brighter optical/UV source, because larger SMBHs produce accretion discs with lower effective temperatures, moving the optical/UV bands up the Rayleigh-Jeans tail and closer to the peak of the multi-colour blackbody spectrum (Lodato & Rossi 2011). The effect of spin on optical/UV emission is strong for a high mass BH, but weak for a low mass BH. This behavior arises because all the optical/UV emission is generated by the disc relatively close to the BH ($R_{\text{out}} \lesssim 20R_g$, $R_g = GM_{\bullet}/c^2$) for discs associated with larger M_{\bullet} , while for a low mass BH, most of the optical/UV emission is generated in a region relatively far from the BH. The colour $u - w2$, based on bands from the *Neil Gehrels Swift Observatory* (Gehrels et al 2004), is roughly 1.1 mag, and it is not very sensitive to M_{\bullet} and a_{\bullet} .

The middle plot shows the light curves for different combinations of M_{\bullet} and R_{out} . Here, we fix $a_{\bullet} = 0.9$. As the disc size increases by a factor of 2, the optical/UV emission brightens by about 1 mag. The larger disc radius increases the disc area by a factor of four, while the UV flux increases² by a factor of ~ 2.5 . As a result, the cooler larger disc also contributes a significant part to the optical/UV emission. Again, the colour $u - w2$ is roughly 1.1 mag, and the value and its evolution are not very sensitive to disc size. Since the disc UV emission follows the Rayleigh–Jeans law, given an accretion rate $\dot{m}_t \propto t^{-n}$ (here, $n=1.53$), the UV light curve decays as,

$$M_{\text{UV}} \propto \frac{2.5n}{4} \log_{10}(t). \quad (1)$$

The left and middle figures show good agreement with the linear relationship between magnitude and time. However, we note that the above relationship is only valid for a disc with constant R_{out} ; if the disc can viscously spread (Cannizzo et al. 1990), then the light curves will decay more slowly with time.

The right panel of Figure 1 shows the effect of viscous disc spreading. As the TDE disc is finite, the accreted debris transfers part of its angular momentum outward through the viscous torque, making the disc spread outwards over time (Cannizzo et al. 1990; Mummery & Balbus 2020). Because of the well-known viscous instability of realistic parametrizations of angular momentum transport in hot accretion flows (Lightman & Eardley 1974), it is not possible to build a self-consistent 1D time-dependent model for a spreading disc dominated by radiation pressure. We instead develop a toy model to estimate the R_{out} of the spreading disc (see Appendix B). In this model, we ignore the specific nature of the viscous torque, and only require conservation of mass and angular momentum. We use Eq. B1 to evaluate the spreading R_{out} at different time. When plotting the figure, we adopt $\Gamma = -3/2$ and use the mass fallback rate to estimate the mass accreted (ΔM) by the BH.

¹ The absorption of disc X-rays by a time-variable absorbing column indicates that *some* reprocessing is occurring; whether or not it is the dominant contributor to the early-time optical/UV emission is an important question we will investigate later in this paper.

² The outer disc is cooler than the inner disc. As the inner hotter disc contributes more optical/UV photons per area than the outer disc, the integrated flux increases more slowly than the disc size as R_{out} grows.

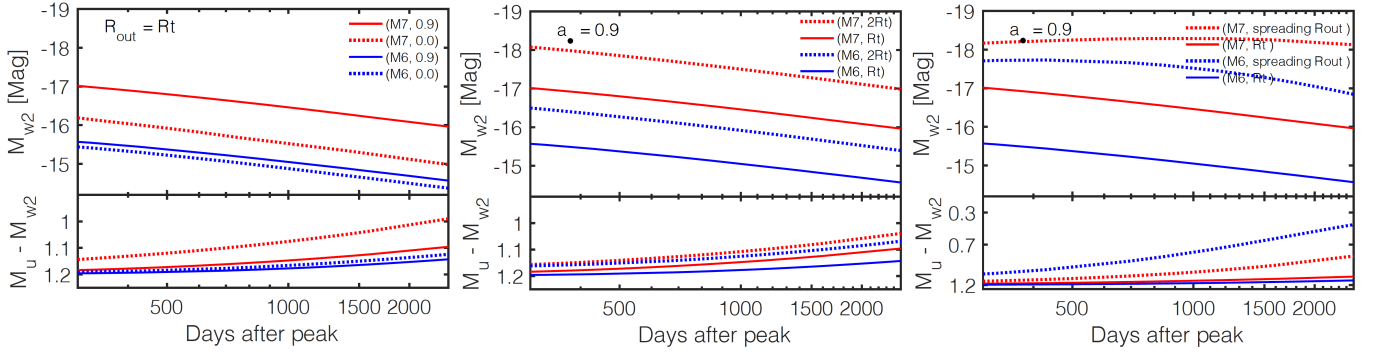


Figure 1. Theoretical thermal slim disc optical/UV light curves for different M_\bullet , a_\bullet , and outer disc radius R_{out} . Here we assume the viewing angle $\theta = 45^\circ$, disc viscosity parameter $\alpha = 0.1$, luminosity distance $d_L = 10$ pc, TDE penetration parameter $\beta = 2$, and progenitor star mass $M_\star = 2M_\odot$ throughout. The left figure shows the light curves for different M_\bullet and a_\bullet , with the outer radius fixed at $R_{\text{out}} = R_t$. The middle figure shows the light curves for different M_\bullet and R_{out} , with $a_\bullet = 0.9$. The right figure considers a viscously spreading disc, but with an independent model for the viscous torque (see Appendix B). In all figures, we use the notation $\text{MX} = 10^X M_\odot$. The upper sub-panels show the light curves in the $w2$ (1928 Å) filter band, and the lower sub-panels show the difference in AB magnitude between the u (3465 Å) and $w2$ bands. The figures show that (1) thermal disc UV emission is brighter for higher M_\bullet , as a higher M_\bullet yields a larger physical disc size; (2) for M_\bullet , a_\bullet , and R_{out} there is a positive correlation between the value of the parameter and the normalisation of the light curve; (3) the spreading disc makes the light curves flatter than those with fixed R_{out} ; (4) the $u - w2$ colour evolution is small (0.1–0.2 mag) over about 2000 days (except for the case of the viscously spreading disc) and it therefore insensitive to the parameters under consideration, e.g., M_\bullet , a_\bullet and R_{out} and \dot{m} (the \dot{m} dependence is implicit as different epochs have different accretion rates). Furthermore, such a colour evolution will be difficult to measure given the typical measurement uncertainties, including those incurred due to subtracting the host galaxy light and uncertainties in the extinction.

The UV light curve of spreading disc is at least 1 mag brighter (after 300 days) than the UV light curve of the disc with fixed R_{out} , and its decay is much flatter. The disc radius R_{out} extends by a factor of 5 and 13 in 2000 days, for case of M7 and M6, respectively. We see the colour also undergoes significant changes (0.5 mag). The precise nature of viscous spreading can place additional constraints on the M_\bullet and a_\bullet estimation, e.g., the UV light curve predicted from the X-ray spectral fits (without a spreading disc) would decay faster than the observed UV light curve.

3 OBSERVED OPTICAL/UV LIGHT CURVES FOR ASASSN-14li

The TDE ASASSN-14li (Holoien et al. 2016) has been monitored for over five years using *Swift*, with the latest observation obtained on December 2, 2020. We reduced all UVOT (Roming et al. 2005) data using the latest calibration files (20201215) and software (heasoft 6.29). Multiple sub-exposures within with the same observation ID are combined in the image plane before applying aperture photometry. The aperture radius is fixed to 5" and a curve of growth aperture correction is applied.

In the latest epochs the UV flux still exceeds the pre-flare baseline, as inferred from the broadband SED of the host galaxy (van Velzen et al. 2021), by about 0.5 mag. About 400 days after the first detection (Brown et al. 2017), the host-subtracted UV light curves flatten to a near-constant plateau (van Velzen, et al. 2019). In this work we focus on this late-time plateau. We apply our models to the difference photometry (i.e., after baseline subtraction) and apply a correction for Galactic extinction.

4 MODELING ASASSN-14li’s LATE-TIME EMISSION

In this section, we fit the late-time UV light curves of ASASSN-14li. The UV light curves are corrected for extinction by neutral gas and dust located in the Milky Way in the line of sight towards ASASSN-14li, but not for any contribution to the extinction from gas and dust located in the host galaxy. As a result, we explore the effect of gas and dust extinction from the host galaxy taking it as a free parameter in our modeling. For simplicity, we assume the same extinction across all late-time epochs. We consider 7 kinds of extinction curves from PYSYNPHOT (STScI Development Team 2013). They are LMC30DOR (Gordon et al. 2003), LMCavg (Gordon et al. 2003), MWDENSE (Cardelli et al. 1989), MWAVG (Cardelli et al. 1989), MWRV21 (Cardelli et al. 1989), MWRV4 (Cardelli et al. 1989), and XGALSB (Calzetti et al. 2000). These models describe three kinds of dust grains environment, e.g. general Milky Way extinction environment (Gordon et al. 2003), diffuse and dense interstellar medium (Cardelli et al. 1989), dust environment in starburst galaxies (Calzetti et al. 2000). The extinction effect for all the 7 models can be described by a single parameter colour excess, E_{B-V} , since the different R_V values are taken into account in the different models.

We refit the X-ray spectra of ASASSN-14li using the slim disc model of W21 (see Appendix A, as well as (Wen et al. 2022)). From the X-ray spectral fits, for a pair of M_\bullet and a_\bullet , we get the best-fit accretion rate at each epoch, as well as the disc inclination. To calculate the UV emission at different epochs, we estimate the accretion rate at each epoch, using the accretion rate decay law obtained through the X-ray spectral fits, and set the disc outer radius R_{out} as a free parameter. However, as the disc may viscously spread with time, we bin the light curves in several bins and allow the fit to the data in each of the different bins to adopt a different R_{out} . We will explore the effect of binning method on the fitted R_{out} in more details in section 4.2 (see Table 1). The free parameters are E_{B-V} and $R_{\text{out},i}$, where i denotes different bins number.

In order to compare the predictions with the *Swift* observations,

we simply compute the magnitude at the central wavelength of each UV filter band. For the four *Swift* bands of interest (w_2 , m_2 , w_1 , u) these are³: $w_2 = 1928 \text{ \AA}$, $m_2 = 2246 \text{ \AA}$, $w_1 = 2600 \text{ \AA}$, and $u = 3465 \text{ \AA}$. We fit the observations using a fit-function comprised of the slim disc model attenuated by extinction. We use the POWELL method (Press et al. 2002) to search for the best fit χ^2 . We quote the 1σ error of each parameter (single parameter) by adopting $\Delta\chi^2 = 1$.

4.1 Successful Fits with a Bare Accretion Disc

Figure 2 shows our best fit to the four observed UV light curves. Here we only fit the late-time epochs denoted with different colours (red, blue, cyan, and magenta). We will come back to the early-time (black) epochs in the next section. In this analysis, we fix M_\bullet , a_\bullet , and the disc inclination at the best-fit values obtained from our X-ray spectral fits, where $10^{+1}_{-7} \times 10^6 M_\odot$, $a_\bullet = 0.998_{-0.7}$ and $\theta = 76^{+4}_{-74}$ (0° means face on). The accretion rate is also a parameter obtained from our X-ray spectral fits. Its evolution can be approximated with the following function: $\dot{m}_t = 231(t + 150)^{-1.04 \pm 0.02}$. Here, t is in days after the first detected by the All Sky Automated Search for Supernova (ASASSN) on MJD 56983.6 in a post-starburst galaxy with $z = 0.0206$ (Jose et al. 2014), and \dot{m}_t is the mass accretion rate in Eddington units with $\dot{M}_{\text{Edd}} = 1.37 \times 10^{15} M_\bullet / M_\odot \text{ kg s}^{-1}$. We note that a different value of M_\bullet and a_\bullet will lead to a somewhat different \dot{m}_t equation (see Appendix A)⁴.

We obtained 13 epochs of UV observations after $t = 350$ d. In order to explore how well the model can fit an observation, we divided them into 4 groups as shown in Figure 2. For epochs within the same group, we assume that they have the same disc outer radius, which we parameterize as R_1 , R_2 , R_3 and R_4 for the 4 groups. In addition to the intrinsic UV emission from the slim disc model, we also employ one of the extinction models mentioned in the first paragraph of Section 4 to account for any host galaxy extinction. Therefore, the free parameters of this analysis are R_1 , R_2 , R_3 , R_4 and E_{B-V} . We note that the fitting result of the parameters are not sensitive to the grouping method (see Table 1).

As can be seen from Figure 2, we successfully fit the four late time UV light curves simultaneously. Interestingly, the fit is only successful if we employ the starburst extinction model *xGALSB* (Calzetti et al. 2000) (we will investigate this in detail in Section 4.2). This shows that the late-time UV emission is consistent with a disc spectrum, which is in line with the results of van Velzen, et al. (2019) and MB20. The reduced χ^2 is $\chi^2/\text{d.o.f} = 69.38/43$, with the first bin deviating the most from the model (hence contributing most to the χ^2). The discrepancy between the model and the data in the first bin may be explained if the UV light at that epoch is a combination of the UV slim disc emission and another source of UV emission.

We also fit the light curves with a power-law model $M_i = k \log_{10}(t + 150) + A_i$, where M_i denotes the magnitude of different bands and A_i is the corresponding fitted intercept. We find a best fit with a reduced $\chi^2/\text{d.o.f} = 63.27/43$ and $M_i \propto (0.97 \pm 0.07) \log_{10}(t + 150)$. The power-law model yields a better fit than that of the slim disc (both altered by an extinction model), likely because in the power-law fit the normalization of each light curve is determined separately, while the normalization of each light curve is associated with the disc spectrum and the extinction model for slim disc fit. The fitted power-law decays faster than that predicted by

the slim disc model, i.e. $M \propto (0.66 \pm 0.03) \log_{10}(t + 150)$ inferred from the $\dot{m}_t = 231(t + 150)^{-1.04 \pm 0.02}$. We note that if we ignore the last two epochs, the fitted power law index is 0.77 ± 0.15 , which is consistent with the predicted value of 0.66 ± 0.03 inferred from slim disc modeling⁵.

The power law index (0.77 ± 0.15) obtained from fitting the late-time UV light curves indicates that, for a fixed R_{out} accretion disc, the disc accretion rate should decay as 1.2 ± 0.2 (see Eq. 1) during the first ~ 1200 days. As the R_{out} will increase due to angular momentum transferring, the real disc accretion rate should decay faster than 1.2 ± 0.2 . For most $\{M_\bullet, a_\bullet\}$ pairs in the 1σ contour (see Figure 6 of W20), the fitted disc accretion rates decay as a power law with index ~ 1.1 , but three cases have an index < 1 , $n = 0.94 \pm 0.01$ for $\{8 \times 10^6 M_\odot, 0.998\}$, $n = 0.90 \pm 0.01$ for $\{7 \times 10^6 M_\odot, 0.998\}$, and $n = 0.95 \pm 0.02$ for $\{5 \times 10^6 M_\odot, 0.8\}$. These three pairs of $\{M_\bullet, a_\bullet\}$, located near the boundary of the 1σ contour, would fall outside the 1σ contour if we included the effect of a spreading disc, since the disc spreading effect will place an additional constraint on the \dot{m} of each epoch. However, how much it improves the constraint on $\{M_\bullet, a_\bullet\}$ is not the focus of this paper.

As the power index (~ 1.1) from the X-ray spectral fits is close to the index 1.2 ± 0.2 inferred from the observed optical/UV light curves (with no disc spreading effect), the viscous spreading of the disc should be slow. If not, the late time disc Optical/UV will be brighter than the observation due to a quick increasing disc size. We will explore this effect in more details in the following section.

4.2 Constraints on Host Extinction and Disc Size

In this section, we will explore whether the host extinction model affects the UV fitting results. Furthermore, we investigate how the other free parameter, the disc radius R_{out} , evolves in time. For the first question, we fit the four UV light curves with the slim disc model attenuated by different extinction models. For the second question, we fit the light curves employing different data groups and different values of the $\{M_\bullet, a_\bullet\}$ pair using the slim disc model (including our fiducial extinction model).

Table 1 shows the fitting results for different extinction models and different data groupings. We first fit the data with the same R_{out} for all epochs and no extinction (row 1). The fits to the data are poor, as the reduced χ^2 values are > 2 and the fitted disc outer radius is $\approx 10.8 R_g$, which is $\approx 1.1 R_t$ ⁶. This is in tension with both the theoretical expectation that $R_{\text{out}} = 2R_t/\beta$ (although it could be explained by a deeply plunging TDE), and also the X-ray spectral fits. As most X-ray photons are generated within $20R_g$ (W20), a much smaller disc size would affect the X-ray spectrum significantly. The (too) small fitted disc size from a model that ignores the effects of extinction on the emergent UV spectrum indicates that host extinction is likely important.

In order to fit the host extinction, we fit the light curves with 7 different extinction curves from PYSYNPHOT (STScI Development Team 2013); see row 2-8 of Table 1. The impact on the UV emission can be described with only one parameter (E_{B-V}) for all the 7 extinction models. From Table 1, one can see that the LMC and MW extinction models do not yield a better fit to the data when compared with no

⁵ As there is no X-ray spectrum available to calibrate the accretion rates after 1200 days, we compare the power law index from slim disc modeling with the power law index from the UV light curves fitting without the last two epochs.

⁶ For $M_\bullet = 10^7 M_\odot$, R_t is about $R_t \approx 10.13 R_g$ for a disruption of a solar-like star with penetration parameter $\beta = 1$.

³ <http://www.swift.ac.uk/analysis/uvot/filters.php>

⁴ Other choices of M_\bullet and a_\bullet lead, however, to very similar fitting results, e.g. $E_{B-V} \sim 0.01$ and $R_{\text{out}} = 2R_t$ (see Fig. 3).

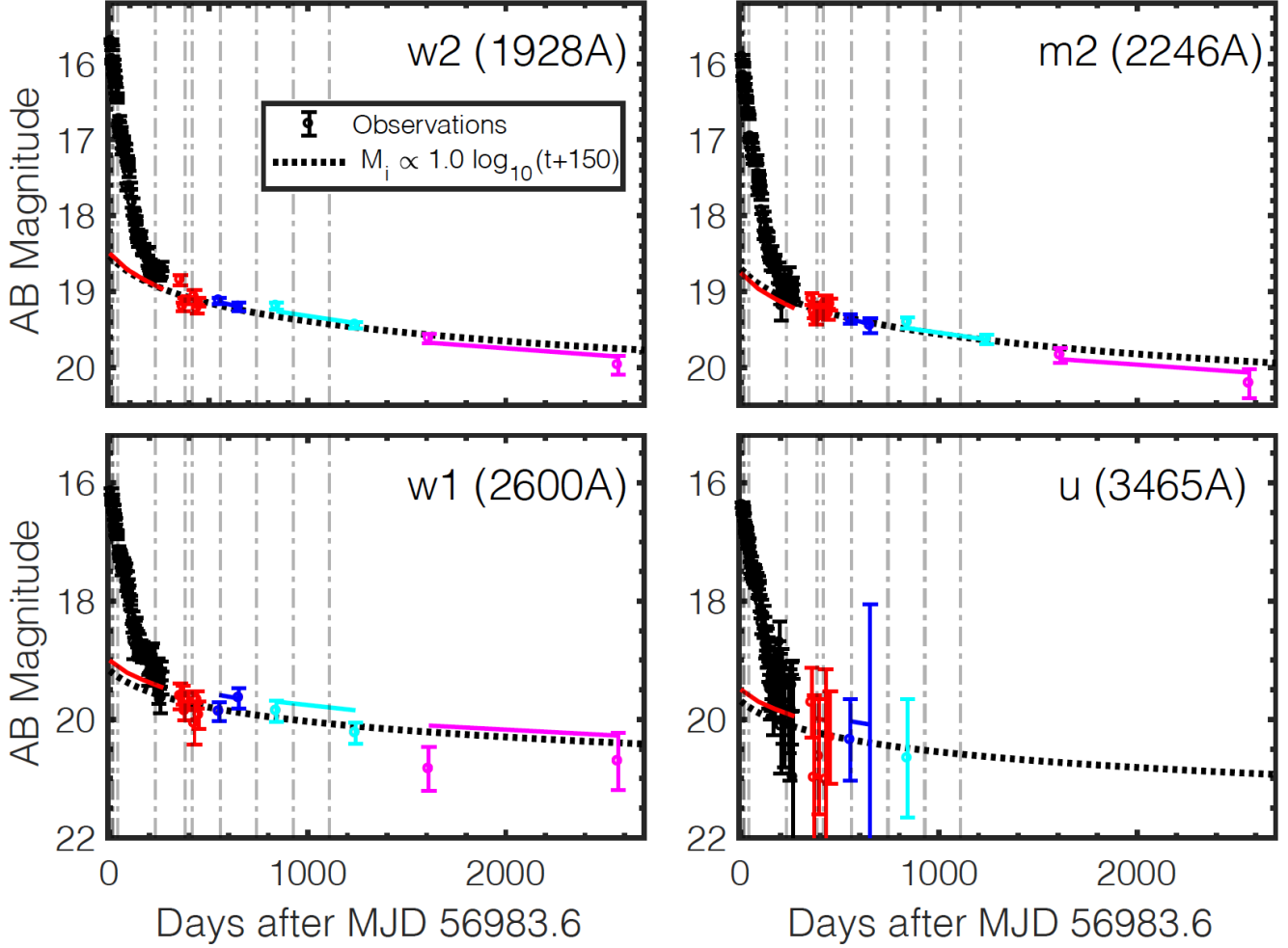


Figure 2. Best fits to the late-time UV light curves in four different optical/UV filter bands obtained through *Swift*/*UVOT* observations. Before the fit, the observed magnitudes have been corrected for extinction due to our own Galaxy, but not for any host extinction. Our approach assumes that there is no additional extinction associated with the TDE itself. The solid lines of 4 different colours denote the best-fit to the late-time (colour) data points using the slim disc model attenuated by a starburst extinction model (Calzetti et al. 2000). The black dotted lines show the best-fit to the data (excluding the black data points at early times) using a simple power-law model. The vertical gray dotted lines show the dates of X-ray observations. For the slim disc plus extinction fit, we fit the data averaged in the four groups denoted by different colours. This figure shows that the late-time UV emission of ASASSN-14li is consistent with the UV emission predicted from a slim disc, where most of the parameters of the slim disc are already determined from the X-ray spectral fits. The fitting results are listed in the *xgalsb₄* row of Table 1.

model for the extinction, as the χ^2 only decrease by ≈ 1 which is not significant given that there is one additional free parameter. Furthermore, the best-fit E_{B-V} values are consistent with 0 at the 1σ confidence level, and the fitted R_{out} is marginally consistent with the value obtained without modeling for the effect of extinction. However, the starburst extinction model results in a better fit with χ^2 decreasing by ~ 12 . The disc size has a best-fit value of $19.2 \pm 1.0 R_g$, which is consistent with $R_{\text{out}} = 2R_t$ ($20.3 R_g$). The fitted $E(B-V)$ is about 0.009 mag. This low value is not a surprise since: (1) surveys show that the value of $E(B-V)$ is within the range of 0.0–1.0 mag often found in starburst galaxies (Calzetti 1997), (2) the low $E(B-V)$ value is consistent with the UV detection of ASASSN 14li, (3) we know that ASASSN-14li occurred in a post-starburst ((Prieto et al. 2016)) galaxy that ended ~ 400 Myr ago (French et al 2017) and that the dust content of such galaxies declines over time (Li et al. 2019).

We now explore the evolution of disc size. In rows *xgalsb₂*, *xgalsb₃*

and *xgalsb₄* of Table 1, we fit the light curves with 2 groups, 3 groups, and 4 groups, respectively. When grouping the data, we always set the last two epochs as a separate group, as the accretion rates of these two epochs cannot be determined independently (there are no X-ray observations at those epochs). For *xgalsb₂*, the χ^2 decreases by about 7 when compared to the best-fit value for the *xgalsb₁* model. The p values obtained from an F-test (James 2020) relative to the 1-group model are 0.05, 0.03, and 0.05, for 2-, 3-, and 4-group models, respectively.⁷ These p values show that the additional groups are only marginally warranted. The ΔAIC (Akaike 1974) relative to a 1-group model are 5.0, 9.0, and 7.5, for 2-, 3-, and 4-group models,

⁷ p is the probability (between 0 and 1) that the improvement of the fit is due to chance. Therefore, a small value of p means a high confidence that the additional parameters are warranted.

Table 1. Results of fits to the late time UV emission of ASASSN-14li. BH mass, BH spin, the disc accretion rate and inclination are fixed at the best-fit value obtained from the X-ray spectral fits (W20). The $\chi^2/d.o.f.$ values show that the use of the model `xgalsb` (i.e., a starburst extinction curve) gives a significantly better fit than any another extinction model we consider, consistent with the post-starburst nature of the ASASSN-14li host galaxy. The final four rows of the table compare the effect of binning of the late-time UV data into different numbers of epochs. We see that the addition of more groups make the fits slightly better, marginally warranting our inclusion of four groups. The fitted radius of the disc is about $2 \times R_t$ ($R_t = 10.13R_g$). Note that, `lmc30dor` (Gordon et al. 2003)— $R_V = 2.76$. `lmcavg` (Gordon et al. 2003)— $R_V = 3.41$. `mwdense` (Cardelli et al. 1989)— $R_V = 5.00$. `mwavg` (Cardelli et al. 1989)— $R_V = 3.10$. `mwr21` (Cardelli et al. 1989)— $R_V = 2.1$. `mwr4` (Cardelli et al. 1989)— $R_V = 4.0$. `xgalsb` (Calzetti et al. 2000)— $R_V = 4.0$.

Extinction model	E_{B-V} [10^{-3} mag]	R_1 [R_g]	R_2 [R_g]	R_3 [R_g]	R_4 [R_g]	$\chi^2/d.o.f$
NA	NA	10.8 ± 0.1	NA	NA	NA	95.05/47
<code>lmc30dor</code>	0.2 ± 0.1	11.1 ± 0.1	93.74/46
<code>lmcavg</code>	0.1 ± 0.1	11.1 ± 0.1	94.43/46
<code>mwdense</code>	0.1 ± 0.1	11.0 ± 0.1	94.68/46
<code>mwavg</code>	0.1 ± 0.1	11.0 ± 0.1	94.61/46
<code>mwr21</code>	0.1 ± 0.1	11.0 ± 0.1	94.56/46
<code>mwr4</code>	0.1 ± 0.1	11.0 ± 0.1	94.63/46
<code>xgalsb1</code>	8.8 ± 0.6	19.2 ± 1.0	82.77/46
<code>xgalsb2</code>	8.7 ± 0.3	19.2 ± 1.0	16.7 ± 1.0	75.71/45
<code>xgalsb3</code>	9.7 ± 0.2	20.0 ± 2.0	21.4 ± 3.0	17.8 ± 2.0	...	69.73/44
<code>xgalsb4</code>	9.8 ± 0.2	20.1 ± 4.1	21.4 ± 3.0	21.9 ± 4.1	17.8 ± 3.0	69.20/43

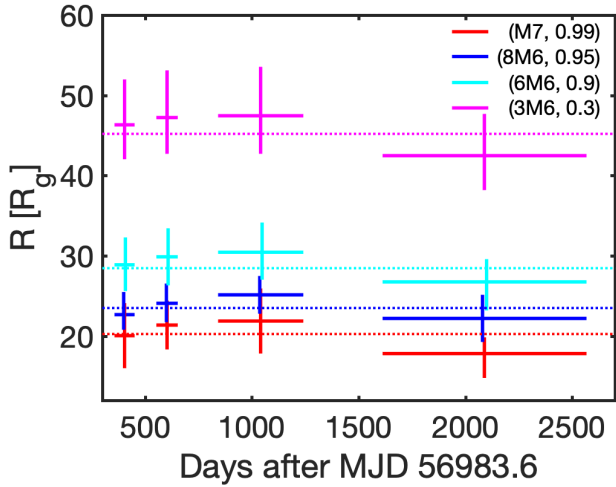


Figure 3. Evolution of R_{out} expressed in unit of R_g for different pairs of $\{M_\bullet, a_\bullet\}$. We fit the UV light curves with a slim disc plus starburst extinction model. The accretion rate and disc inclination are fixed at their best-fit value from X-ray spectral fitting. The dotted color lines show $R_{\text{out}} = 2R_t$, respectively. We find that R_{out} is consistent with a constant value at the 1σ confidence level, for all four cases, challenging the baseline expectation of a viscously spreading disc.

respectively⁸. These ΔAIC values also show that adding more data bins is not strongly preferred. These two tests show that there is no strong evidence for evolution of R_{out} at different times. This can be also seen from the fitted radii of the 4-group model (see also Fig. 3). In each of the 4 temporal groups, the outer radius is consistent with $2R_t$ at a 1σ level.

Figure 3 plots the fitted R_{out} for different pairs of M_\bullet and a_\bullet . As one can see the fitted R_{out} is consistent with a constant value at the 1σ confidence level for all cases considered. In each case, the fitted R_{out} is consistent with $2R_t$. As the debris is accreted, it will transfer part

⁸ $\Delta\text{AIC} = \Delta\chi^2 + 2\Delta K$, where K is the number of free parameters. Generally speaking, two models with $\Delta\text{AIC} = 5$ and 10 are considered to present strong and very strong evidence, respectively, against the weaker model.

of its angular momentum to the outer disc, which (absent additional physics) will result in viscous expansion.

However, our fits find significantly less viscous spreading than would be expected in simple models. This could signify that either (1) the majority of the bound debris remains unaccreted in a low-viscosity disc at late epochs, or (2) significant amounts of disc angular momentum have been expelled from the system during the circularization⁹ or accretion process. The latter possibility may be the most natural; angular momentum loss in a magnetized wind has been predicted in both analytic (Blandford & Payne 1982; Ferreira & Pelletier 1995) and numerical (Scepi et al. 2018) magnetohydrodynamics.

In general, our fits show that, 1) only a starburst extinction curve can give a better and more reasonable fit to the observed optical/UV light curves, 2) the disc size is about $2R_t$, and is consistent with a constant at the 1σ CL.

5 IMPLICATIONS OF ASASSN-14li’s EARLY-TIME OPTICAL/UV LIGHT CURVES

As is shown in Figure 2, the early time UV emission is at least 10 times brighter than the predicted near-UV emission from our slim disc fits (which peak at ~ 0.1 keV) to early time X-rays. On the other hand, the bolometric early time disc luminosity is > 10 times brighter than the luminosity derived from the early time blackbody near-UV emission (see Fig.4). These two factors indicate that there should be another thermal photosphere, with a lower effective temperature ($\sim 3 \times 10^4$ K) but much larger emitting area than the disc, in order to account for the early UV emission. The origin of this large-scale, early time photosphere (which is typical of optically selected TDEs) has been the subject of much theoretical debate; see (Roth et al. 2020) for a recent review.

The rich X-ray dataset available for ASASSN-14li allows us to test competing models for early-time optical/NUV emission in greater detail than is possible for most other TDEs observed to date. In this Section, we present a set of self-consistency checks that can be employed to check the validity of (i) shock-powered early-time emission (Piran et al. 2015; Shiokawa et al. 2015; Steinberg & Stone

⁹ See e.g. (Bonnerot & Lu 2020) for an interesting example of how circularization may preferentially expel matter in one direction, dramatically changing the angular momentum budget of the remaining bound material.

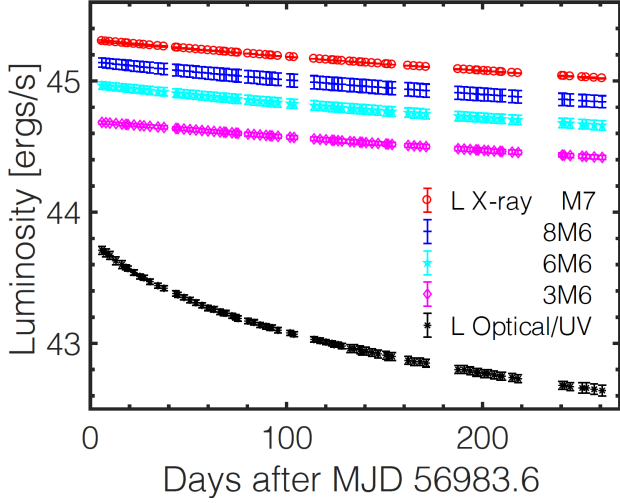


Figure 4. The early time bolometric luminosity derived from slim disc modeling and the blackbody Optical/UV emission. For the bolometric luminosity inferred from X-ray spectral fitting, we estimate \dot{m} at each Optical/UV epoch by using the decay of accretion rate from X-ray spectra fitting.

2022); (ii) reprocessing of X-ray/EUV photons by an outflowing wind (Metzger & Stone 2016; Roth & Kasen 2018; Lu & Bonnerot 2019; Piro & Lu 2020); and (iii) reprocessing of X-ray/EUV photons by a quasi-static photosphere (Loeb & Ulmer 1997; Coughlin & Begelman 2014; Guillochon et al. 2014; Roth et al. 2016). The test of the shock-powered emission mechanism is entirely novel, while the tests of the two variants of the reprocessing paradigm follow a similar line of reasoning as in the work of (Matsumoto & Piran 2021).

5.1 Emission from a Self-Intersecting Shock

In W20, we first presented detailed, time-dependent fits to the XMM-Newton spectra of ASASSN-14li, which have been slightly updated here. We can now combine this time-dependent estimate for the ionizing continuum produced by the inner disc with independent optical/NUV light curves (Holoien et al. 2016; Brown et al. 2017) to pose a simple geometrical question. The optical/NUV light curves of ASASSN-14li imply an emitting area which can be measured directly under the assumption of a blackbody spectrum. In the simplest version of the shock paradigm, the radial location of the optical/NUV photosphere is linked to the physical position of the stream self-intersection shocks, and therefore we may determine the total solid angle subtended by the optical/NUV photosphere (from the perspective of the central accretion disc). This occluded solid angle, in combination with the ionizing continuum of the central disc, determines a characteristic reprocessing luminosity which must be significantly less than the observed optical/NUV luminosity in order for shock-powered emission to provide a self-consistent model.

To make the above self-consistency check more quantitative, we will consider a star of mass M_\star and radius R_\star disrupted by a SMBH of mass M_\bullet (and spin a_\bullet). Tidal disruption occurs if the star's pericenter R_p is less than the tidal radius (Rees 1988)

$$R_t = R_\star \left(\frac{M_\bullet}{M_\star} \right)^{1/3}. \quad (2)$$

Equivalently, disruption occurs if $\beta = R_t/R_p > 1$. The elongated debris streams produced following disruption fly out to a large range

of radii before returning to pericenter (Stone et al. 2013; Guillochon & Ramirez-Ruiz 2013); the semimajor axis of the most tightly bound debris is

$$a_{\min} = \frac{R_t^2}{2R_\star} = \frac{R_\star}{2} \left(\frac{M_\bullet}{M_\star} \right)^{2/3}. \quad (3)$$

Shocks will be generated by the self-intersection of debris streams¹⁰, at a radius R_{SI} . If the unfortunate star had a highly relativistic pericenter, apsidal precession will force self-intersections at $R_{\text{SI}} \ll a_{\min}$, while a less relativistic pericenter will result in quasi-apocentric self-intersections¹¹ at $R_{\text{SI}} \approx a_{\min}$ (Dai et al. 2015). More precisely, the debris stream longitude of pericenter ω will, at leading post-Newtonian order, shift by an amount (Merritt et al. 2010)

$$\delta\omega = A_S - 2A_J \cos \iota \quad (4)$$

per orbit (with most of the apsidal shift occurring during pericenter passage). Here ι is the spin-orbit misalignment angle, and the individual terms in this equation are

$$A_S = \frac{6\pi}{c^2} \frac{GM_\bullet}{R_p(1+e)} \approx 11.5^\circ \left(\frac{\tilde{R}_p}{47.1} \right)^{-1} \quad (5)$$

$$A_J = \frac{4\pi}{c^3} a_\bullet \left(\frac{GM_\bullet}{R_p(1+e)} \right)^{3/2} \approx 0.788^\circ \left(\frac{\tilde{R}_p}{47.1} \right)^{-3/2} a_\bullet, \quad (6)$$

representing the leading-order contributions of the SMBH mass and spin, respectively. Note that $\tilde{R}_p = R_p/R_g$ is a dimensionless pericenter normalized by the gravitational radius ($R_g = GM_\bullet/c^2$), and e is the eccentricity of the debris streams (typically, $0.99 < e < 1$). From the above equations we see that the contribution of SMBH spin a_\bullet to $\delta\omega$ is always highly sub-dominant for $\tilde{R}_p \gtrsim 10$ and therefore we neglect it in the remainder of this calculation. The apsidal shift $\delta\omega$ causes stream self-intersection at the radius (Dai et al. 2015)

$$R_{\text{SI}} = \frac{R_p(1+e)}{1+e \cos(\pi + \delta\omega/2)}. \quad (7)$$

Under the assumption that the photosphere is located near the location of the shocks, the total area of the celestial sphere at the photospheric radius will be $A_{\text{SI}} = 4\pi R_{\text{SI}}^2$.

Under the standard assumption that observed optical/UV emission is a thermal blackbody, we may combine multiband photometric observations to estimate the *true* area of the optical photosphere, $A_{\text{bb}} = L_{\text{bb}}/(\sigma_{\text{SB}} T_{\text{bb}}^4)$. Here σ_{SB} is the Stefan-Boltzmann constant, and L_{bb} and T_{bb} are the observationally inferred blackbody luminosity (bolometric) and temperature. We now compute the covering fraction

$$f_A(t) = \frac{A_{\text{bb}}(t)}{A_{\text{SI}}} = \frac{A_{\text{bb}}(t)}{4\pi R_{\text{SI}}^2}, \quad (8)$$

which in turn can be used to relate the central ionizing luminosity L_{disc} to the time-dependent reprocessing luminosity

$$L_{\text{rep}}(t) = f_A(t) L_{\text{disc}}(t). \quad (9)$$

¹⁰ In the recent simulations of (Steinberg & Stone 2022), shock-powered light curves are driven by dissipation at radii much smaller than R_{SI} , but as we shall see, such a situation would only *strengthen* the constraints derived in this sub-section.

¹¹ Note that this picture may be complicated if relativistic nodal precession is sufficient to prevent immediate stream self-intersections (Guillochon & Ramirez-Ruiz 2015; Hayasaki et al. 2016). Even in this case, however, most of the bound debris would orbit on trajectories with $a \sim a_{\min}$.

We now have two related (but distinct), non-trivial, multi-epoch self-consistency checks for the shock paradigm. Shock-powered emission will not be self-consistent if $f_A \gg 1$, nor if $L_{\text{rep}}(t) > L_{\text{bb}}(t)$. The former inconsistency would imply that the observed optical/NUV photosphere is much larger than plausible self-intersection radii (and as a result, plausible shock dissipation sites will not be able to produce the observed black body radiation). In principle one could accommodate this by positing that the post-shock material must expand significantly before trapped photons can escape, but in practice this will reduce the theoretical shock-powered luminosity below what is observed (due to adiabatic degradation). The latter inconsistency would imply that the observed ionizing continuum, in combination with the observed optical/NUV photosphere, will naturally produce the observed optical/NUV luminosity through reprocessing alone.

These consistency checks depend on both time-dependent quantities, such as $L_{\text{disc}}(t)$, $L_{\text{bb}}(t)$, and $T_{\text{bb}}(t)$ and also inferred (or assumed) parameters of the TDE: M_\bullet , β , M_\star , and R_\star . We use our X-ray spectral modeling from W20 to estimate ranges of M_\bullet , and the associated $L_{\text{disc}}(t)$ curves (which will change as M_\bullet changes). R_\star is determined from M_\star using main sequence mass-radius relationships (Kippenhahn & Weigert 1990), and M_\star is left as a free parameter. We note that UV emission line ratios provide significant constraints on the mass of the ASASSN-14li progenitor star due to the impact of CNO-cycle burning (Kochanek 2016; Yang et al. 2017), and this reasoning has been used to argue that the progenitor of ASASSN-14li was at least $\approx 1.3M_\odot$ (Mockler et al. 2022). However, from the decay rate of \dot{m} (see Fig.A2), it is difficult to determine whether this star is fully or partially disrupted. In addition, from the late time Optical/UV light curves fitting, we get $R_{\text{out}} \sim 2R_t$ (see Fig.3). These two factors indicate that $\beta \sim 1$ is highly possible. As a result, we take $\beta = 1$ ($R_p = R_t$) as an assumption (if β were still larger, the consistency checks would become harder to satisfy).

To test the self-consistency of the shock paradigm, we require $f_A \leq 1$ (Eq. 8) and $L_{\text{rep}} \leq L_{\text{bb}}$ (Eq. 9). We use these upper limits on f_A and L_{rep} to place lower limits on the unknown mass of the victim star, M_\star . For ASASSN-14li¹², the second self-consistency test ($L_{\text{rep}} \leq L_{\text{bb}}$) is at all epochs more constraining than the first ($f_A \leq 1$), due to the fact that $L_{\text{disc}} \gg L_{\text{bb}}$. We show the resulting lower limits on M_\star in Fig. 5. As the absolute strongest constraints on the shock paradigm come from the earliest epochs, we present these alone in Fig. 6.

We see that the self-consistency of the shock paradigm is most constrained by early-time observations ($t \lesssim 100$ days after detection). The resulting lower limits are a sensitive function of SMBH mass. The most generous lower limits are achieved for the smallest SMBHs; at the bottom end of the 1σ confidence limit on M_\bullet ($10^{6.5}M_\odot$), the shock paradigm is self-consistent provided so long as $M_\star \gtrsim 1.4M_\odot$, which is plausible. Conversely, in the upper half of the 1σ CL SMBH mass region ($M_\bullet \gtrsim 10^{6.75}M_\odot$), the shock paradigm requires $M_\star \gtrsim 10M_\odot$, necessitating a very rare TDE which is unlikely to occur in the small present-day TDE sample.

5.2 Emission from a Reprocessing Layer

In this section, we will test whether the early optical/UV emission can be produced by a reprocessing layer of gas. As the disc luminosity is > 10 times brighter than the optical/UV black body luminosity, the putative reprocessing layer is either optically thin (reprocessing only

a small fraction of the photons), or optical thick but only covering a small fraction of the emitted sphere. However, as observations of TDE optical/UV emission are generally consistent with optically thick thermal emission (Dai et al. 2018; Roth et al. 2016), we only consider the latter possibility, and follow the work of Matsumoto & Piran (2021) to estimate how much mass is required to support such a reprocessing layer. As before, we assume an optically thick reprocessing layer with a covering fraction

$$f_A(t) = \frac{L_{\text{bb}}(t)}{L_{\text{disc}}(t)}. \quad (10)$$

Such a gas layer can be produced by outflowing material, either from a super-Eddington disc wind or from the result of shocks in stream-stream or stream-disc collisions (Metzger & Stone 2016; Roth & Kasen 2018; Dai et al. 2018; Lu & Bonnerot 2019). Alternatively, it can be formed from bound but poorly circularized debris (Loeb & Ulmer 1997; Guillochon et al. 2014; Roth et al. 2016). Here we estimate the mass required for both outflowing and quasi-static reprocessing layer models in ASASSN-14li. Our aim is to determine whether reprocessing models can operate within the mass budget provided by the disruption of a plausible star (i.e. $\lesssim 1M_\odot$).

5.2.1 Outflowing Debris Layer

We follow the work of Matsumoto & Piran (2021) to estimate the mass of the outflowing material with different speeds. We note that similar models (Metzger & Stone 2016; Roth & Kasen 2018) have been developed for cases of high speed outflowing material ($\sim 10,000\text{km/s}$). We introduce two critical radii to understand the emergent spectrum, as in (Shen et al. 2015). The first is the thermalization radius, r_{th} , below which the radiation can reach local thermal equilibrium with the gas. We note that the thermalization radius is larger than the radius corresponding to the observed luminosity and black body temperature ($r_{\text{bb}} = \sqrt{L_{\text{bb}}/(4\pi\sigma_{\text{SB}}T_{\text{bb}}^4)}$), due to the fact that the electron scattering optical depth $\tau_{\text{es}} > 1$ (Roth et al. 2016). At this radius, the effective absorption depth, τ_{eff} , is equal to unity (Rybicki & Lightman 1979)¹³:

$$\tau_{\text{eff}}(r_{\text{th}}) = \int_{r_{\text{th}}}^{r_o} \rho(r) \sqrt{3\kappa_a(\kappa_a + \kappa_{\text{es}})} dr = 1, \quad (11)$$

here, $\kappa_{\text{es}} \approx 0.35 \text{ cm}^2 \text{ g}^{-1}$ is the Thomson electron scattering opacity, r_o is the outer edge of the layer, and κ_a is the absorption opacity. In order to derive r_{th} , we use Kramer's law to approximate the absorption opacity,

$$\kappa_a = \kappa_0 \frac{\rho(r)}{\text{g/cm}^3} \left(\frac{T}{\text{K}} \right)^{-7/2} \text{ cm}^2 \text{ g}^{-1}, \quad (12)$$

where κ_0 is a constant which also contains the dependence on the gas composition. Following Matsumoto & Piran (2021), we set $\kappa_0 = 4.0 \times 10^{25}$ for TDEs, a normalization which is consistent with more precise calculations of the Planck mean absorption opacity at Solar metallicity.

The second critical radius is the photon trapping radius r_{tr} , above which the photon diffusion time is shorter than the dynamical time

¹² For a different TDE with a lower disc luminosity, the $f_A \leq 1$ consistency check could be the more constraining of the two.

¹³ While τ_{eff} is properly defined as a frequency-dependent variable, the photons around the Wien peak dominate the luminosity (Rybicki & Lightman 1979). We follow the work of (Shen et al. 2015) and define τ_{eff} to be the effective optical depth of the photons near the Wien peak.

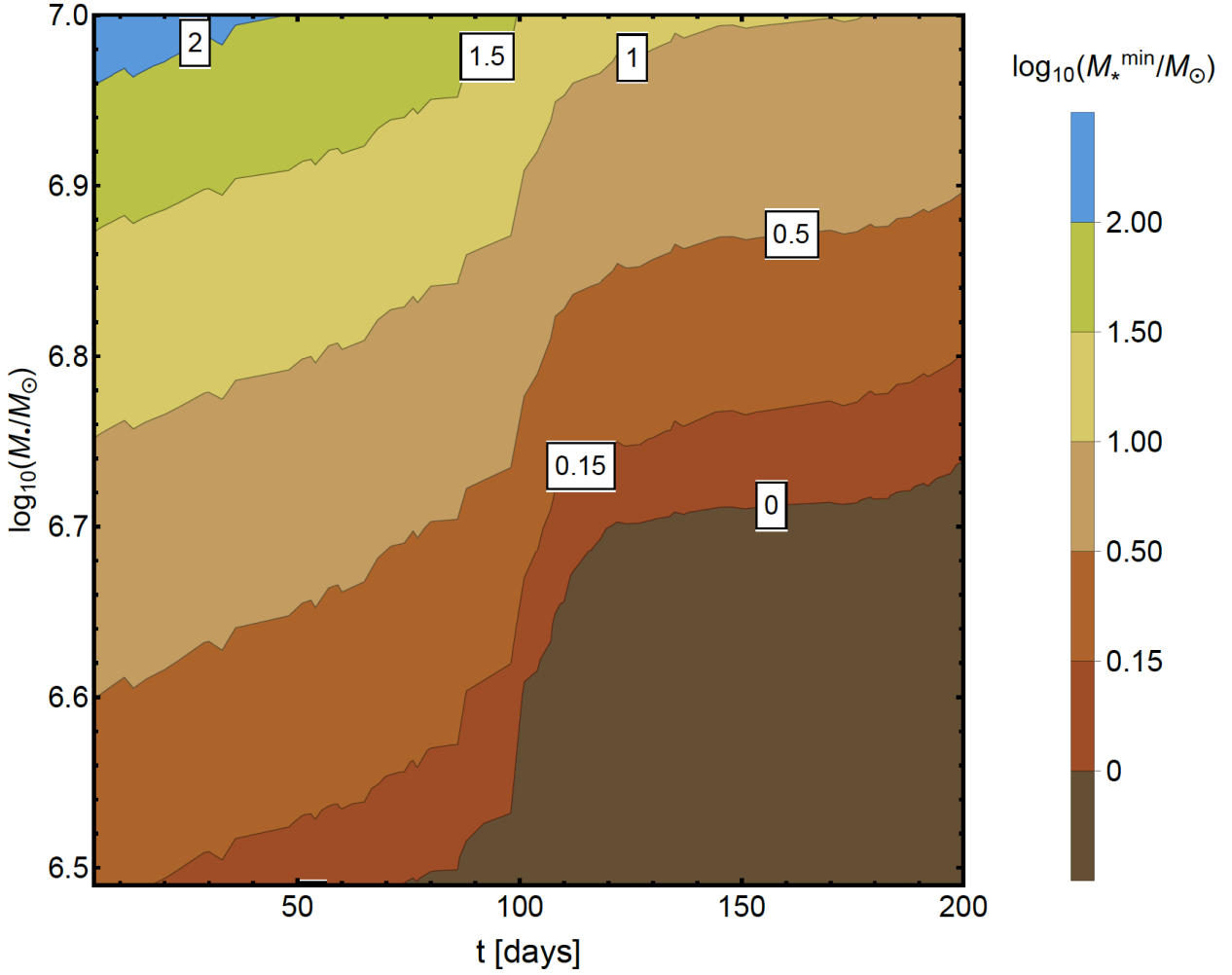


Figure 5. Contours indicating the *minimum* mass of the disrupted star, M_* , required for the shock paradigm to provide a self-consistent description of early-time optical emission. Contours are colour-coded and labeled in terms of $\log_{10}(M_*/M_\odot)$. Different minimum masses are required at different observing epochs (shown on the x-axis as time since first observations), and the minimum mass also depends on the SMBH mass M_\bullet , which is constrained by X-ray continuum fitting to the range shown on the y-axis (at a 1σ confidence level). The minimum mass of the disrupted star required for self-consistency of the shock paradigm at all times is $M_* \approx 10^{0.15} M_\odot \approx 1.4 M_\odot$. Unrealistically massive stars are needed if $M_\bullet \gtrsim 10^{6.7} M_\odot$.

and photons can freely escape from the outflowing material. This radius is defined as,

$$\tau(r_{\text{tr}}) = \int_{r_{\text{tr}}}^{r_0} (\kappa_a + \kappa_{\text{es}}) \rho dr = \frac{c}{v_w}, \quad (13)$$

where c is the speed of light and v_w is the wind speed (at r_{tr}). When $r_{\text{tr}} > r_{\text{th}}$, the photons are trapped with the outflowing material until reaching r_{tr} . As a result, the observed luminosity and observed black body temperature are given by the diffusion luminosity and gas temperature at r_{tr} , respectively.

We now model the density $\rho(r)$ at r_{tr} and r_{th} . As in (Matsumoto & Piran 2021), we consider a steady wind outflow of constant speed v_w , but unlike most earlier analytic work, we assume a covering factor f_A that may be less than unity. More specifically, we assume that the outflow fills a solid angle on the sky that is $\Delta\Omega = 4\pi f_A$, and therefore the density profile along a ray is

$$\rho(r) = \frac{\dot{M}_{\text{wind}}}{4\pi r^2 v_w f_A}. \quad (14)$$

As $\kappa_a \ll \kappa_{\text{es}}$ for TDE photospheres (Roth et al. 2016) and the density

decays faster than r^{-1} in a general outflow, we approximate the radial optical depth in Eq. 11 and Eq. 13 as,

$$\tau_{\text{eff}}(r_{\text{th}}) \approx \sqrt{3\kappa_a \kappa_{\text{es}} \rho_{\text{th}} r_{\text{th}}} = 1, \quad (15)$$

$$\tau(r_{\text{tr}}) \approx \kappa_{\text{es}} \rho_{\text{tr}} r_{\text{tr}} = \frac{c}{v_w}. \quad (16)$$

Assuming thermal equilibrium between photons and the gas, and applying the diffusion approximation, the gas temperature at a given radius in a spherically symmetric outflow can be described as,

$$\frac{d(T^4)}{dr} = -\frac{3\kappa_{\text{es}} \rho(r)}{16\pi \sigma_{\text{SB}} r^2} L_{\text{disc}}(t). \quad (17)$$

We use $L_{\text{disc}}(t)$ instead of $L_{\text{bb}}(t)$ because the covering factor f_A that we consider may be less than unity. We note that the prior equation is only strictly valid in the limit of spherical symmetry, and may break down due to anisotropic photon diffusion in non-spherical systems with $f_A \ll 1$ (in this case Eq. 17 will overestimate the temperature at a given radius).

Taking the approximation $d(T^4)/dr \approx -T_{\text{bb}}(t)^4/r$ at $r = r_{\text{tr}}$ (or at

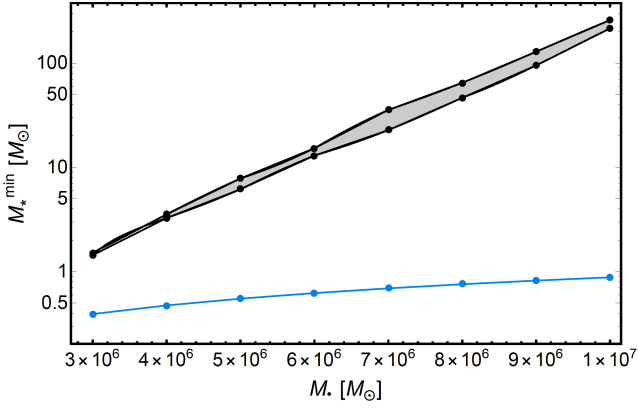


Figure 6. Minimum stellar mass, M_{\star}^{\min} , required for the shock paradigm to be self-consistent. The self-consistency requirement that $L_{\text{rep}} \leq L_{\text{bb}}$ at all observing epochs is shown in black (shaded error region corresponds to the range of permitted SMBH spins at each mass found via X-ray fitting), and the weaker requirement that the photosphere covering fraction $f_A \leq 1$ at all epochs is shown in blue. Both constraints are shown at their strongest, i.e. in the earliest epochs. Reasonable stellar masses (i.e. $\lesssim 3M_{\odot}$, as should be typical for a post-starburst host) allow self-consistency when the SMBH mass is smaller, but a large portion of the 1σ CL on M_{\bullet} (obtained from disc continuum fitting) can be ruled out if the shock paradigm is the true origin of optical/NUV luminosity in ASASSN-14li.

$r = r_{\text{th}}$) and using Eqs. 15 and 16, we get the outflow rate

$$\dot{M}_{\text{wind}} = \begin{cases} f_A(t)^{\frac{1}{5}} L_{\text{bb}}(t)^{\frac{4}{5}} T_{\text{bb}}(t)^{-\frac{11}{10}} v_w \left(\frac{3\pi\kappa_{\text{es}}}{26\sigma_{\text{SB}}^4\kappa_0^3} \right)^{\frac{1}{5}}, & \text{if } v < v_c, \\ f_A(t)^{\frac{1}{2}} L_{\text{bb}}(t)^{\frac{1}{2}} T_{\text{bb}}(t)^{-2} v_w^{-\frac{1}{2}} \left(\frac{3\pi c^3}{\sigma_{\text{SB}}\kappa_{\text{cs}}^2} \right)^{\frac{1}{2}}, & \text{if } v > v_c. \end{cases} \quad (18)$$

Here, the critical velocity, v_c , as determined by $r_{\text{th}} = r_{\text{tr}}$, can be estimated as

$$v_c = f_A(t)^{\frac{1}{5}} \left(\frac{48\pi\sigma_{\text{SB}}\kappa_0^2 c^5}{\kappa_{\text{cs}}^4} \right)^{\frac{1}{5}} L_{\text{bb}}(t)^{-\frac{1}{5}} T_{\text{bb}}(t)^{-\frac{3}{5}}. \quad (19)$$

We note that the \dot{M} and v_c derived here are different from those in Matsumoto & Piran (2021) by a factor of $f_A(t)^{1/5}$ (or $f_A(t)^{1/2}$), primarily due to the covering factor¹⁴.

The mass lost by outflowing material, from the discovery day (t_d) to the current epoch t , can be calculated as,

$$M_{\text{wind}} = \int_{t_d}^t \dot{M}_{\text{wind}} dt'. \quad (20)$$

Figure 7 shows the mass lost by outflow for different wind velocities varying from 4×10^2 km/s to 4×10^4 km/s. The estimated amount of mass lost peaks at the critical velocity of $v_w \sim 10^4$ km/s for which $r_{\text{th}} = r_{\text{tr}}$ and it decreases with increasing M_{\bullet} . This is because a higher M_{\bullet} yields a larger disc, which in turn implies a brighter L_{disc} , which makes the covering factor smaller. The maximum of the amount of mass lost of each curve varies between 0.6 and $1.1 M_{\odot}$, which is somewhat smaller than the \sim few M_{\odot} derived by Matsumoto & Piran (2021). This difference is mainly caused by the covering factor. In this work, we found that the disc luminosity is > 10 times brighter

¹⁴ There is also a factor of 3 in the definition of effective optical depth.

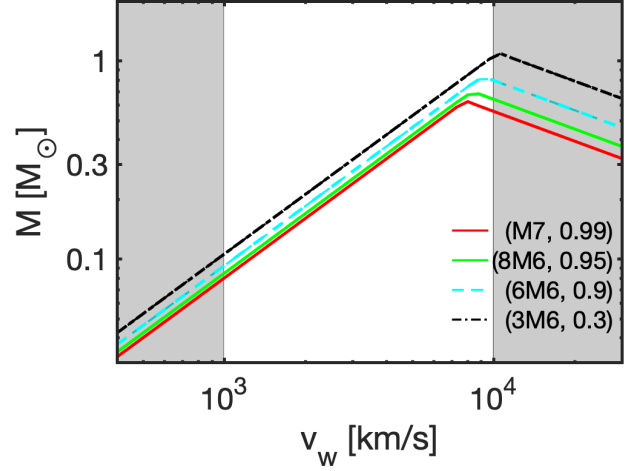


Figure 7. Mass lost by outflowing material for different velocities. The gray shaded regions show velocities excluded by the observations of line widths $v_w < 10^4$ km/s (Arcavi et al. 2014) or lower than the escape velocity $v_w \sim 10^3$ km/s. Even though the full width at half maximum (FWHM) of the line is likely determined by effects of electron scattering, the velocity determined by the FWHM can not be lower than the outflow velocity. The peak of each line denotes $v_w = v_c$.

than the observed optical/UV black body luminosity at peak, which indicates $f_A(t_p) < 0.1$, while Matsumoto & Piran (2021) assume $f_A(t) = 1$ ($L_{\text{disc}} = L_{\text{bb}}$). As the amount of mass lost is between $\sim 0.1 M_{\odot}$ and $\sim 1.1 M_{\odot}$, we cannot rule the outflow model using the optical/UV emission, given that it is conceivable that a star of several solar mass was disrupted in the TDE. Instead, if we take the wind velocity as the escape velocity at r_{th} ($\sim 2 \times 10^3$ km/s), the amount of mass lost to the outflow is $< 0.3 M_{\odot}$, which is less than half of the debris for a TDE of a solar-like star. The main caveat to this calculation is our approximate treatment of photon diffusion in cases with $f_A \ll 1$, which we hope to re-examine with a more detailed calculation in the future.

5.2.2 Static Debris Layer

Turning now to a quasi-static reprocessing layer, we approximate its radial density profile as a power-law,

$$\rho(r) = \frac{K}{r^p} = \frac{M_s(3-p)}{4\pi(r_o^{3-p} - r_i^{3-p})r^p}, \quad (21)$$

where K is a normalization constant, M_s is the layer mass if $f_A = 1$, and p is expected to vary between 1.5 and 3 (Coughlin & Begelman 2014). If $p = 3$, $M_s = 4\pi K \ln(r_o/r_i)$.

For the model involving a static layer of material, the trapping radius is not defined, as the gas has no bulk (outflow) motion. Observations can thus be characterized solely by the thermalization radius. We use the simplified Eq. 15 to describe the effect of the optical depth at r_{th} . The observed optical/UV black body luminosity can be also described by the diffusion approximation as shown in Eq. 17. By assuming $\frac{d(T^4)}{dr} \approx -\frac{T_{\text{bb}}(t)^4}{r}$ at $r = r_{\text{th}}$, we get

$$K = (3\kappa_{\text{es}})^{\frac{2p-3}{5}} \kappa_0^{\frac{-1-p}{5}} (16\pi\sigma_{\text{SB}})^{\frac{2-3p}{5}} L_{\text{disc}}(t)^{\frac{3p-2}{5}} T_{\text{bb}}(t)^{\frac{23-17p}{10}}. \quad (22)$$

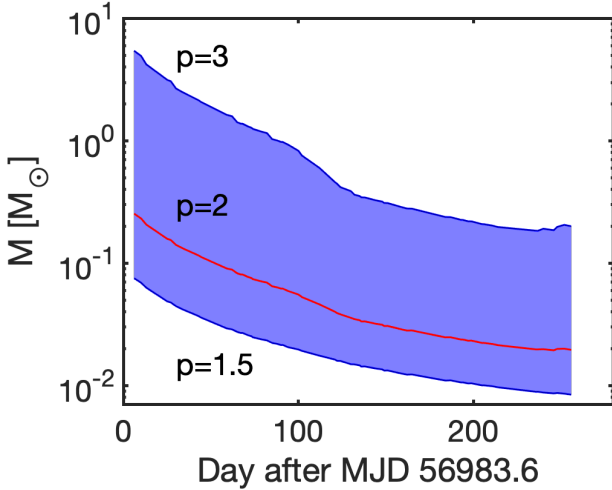


Figure 8. Mass of the static layer as a function of time. Here, we set $r_{\text{out}} = 1.7 \times 10^{15}$ cm (Loeb & Ulmer 1997), estimated by assuming constant ratio of gas pressure to total pressure for radiation supported layer. The mass in the static layer can be $\sim 0.5M_{\odot}$, indicating that the static layer model to explain the optical/UV emission is not ruled out given that it is not inconceivable that a solar mass star was disrupted in the TDE.

The required mass of the layer at each epoch is,

$$M_{\text{static}} = f_A(t)M_s. \quad (23)$$

We set the inner radius of the layer as $r_i = 2r_t$ (typically $\sim 10^{13}$ cm for a $10^6 - 10^7 M_{\odot}$ BH), and $r_{\text{out}} \sim 10^{15}$ cm (Loeb & Ulmer 1997; Coughlin & Begelman 2014; Guillochon et al. 2014).

Figure 8 shows the constraints on the mass of the gas for the static layer. The plot shows that the mass of the layer decreases with time, due to the quickly decreasing optical/UV luminosity. The mass also decreases with increasing M_{\bullet} , because a higher M_{\bullet} results in a brighter L_{disc} , which in turn makes the covering factor smaller. As the maximum mass in the static layer is $\sim 0.5M_{\odot}$, we cannot rule the static layer model out.

6 CONCLUSIONS

We have explored whether a TDE’s optical/UV emission at late times—defined as times after the initial power-law decline of the light curve, and typically hundreds of days after discovery—can be described through quasi-thermal emission from a slim accretion disc. We examined how theoretical disc emission predictions are affected by the SMBH mass, SMBH spin, and an evolving outer disc radius. Applying slightly updated results (see Wen et al. (2022)) from our earlier slim disc modeling of ASASSN-14li’s multi-epoch X-ray spectra (W20), we tested if it is possible to fit the late-time *Swift* u -, $w1$ -, $m2$ -, and $w2$ -band luminosities with only the host interstellar extinction and the time-dependent outer disc radius as free parameters. To better understand the *early*-time optical/UV light curves, we explored constraints on two leading models explaining this emission: (1) shock power arising from self-intersecting debris streams and (2) the reprocessing of obscured, inner-disc X-ray emission by an outflowing or static debris layer.

Our findings are:

- (i) The synthetic optical/UV slim disc luminosity depends on the inclination, the mass accretion rate, the SMBH mass and spin, and outer

disc radius. We fixed the disc inclination to its best-fit value, and we fixed the mass accretion rate as a function of time to that found from the X-ray spectral fits. Expanding the outer disc edge increases the disc’s emitting area and so increases the light curve normalization. Increasing the SMBH mass (while holding the X-ray luminosity constant) decreases the disc temperature, shifting more of its total luminosity into longer wavelengths and increasing the optical/UV luminosity. Increasing the spin (while holding the X-ray luminosity constant) increases the total radiative efficiency of the disc and thus modestly increases the optical/UV luminosity; this effect is generally weak except at the highest masses where the disc is much smaller in dimensionless gravitational radii. Viscous spreading makes the light curves decay more slowly, but this effect weakens for larger M_{\bullet} , where spreading times are longer.

- (ii) The optical/UV luminosities across all four bands depend similarly on the black hole mass, black hole spin, and disc outer radius. Therefore, optical/UV colour (e.g., $u - w2$) is roughly constant with time and is insensitive to M_{\bullet} , a_{\bullet} , and the disc radius, as well as to the accretion rate. The one exception to this conclusion is if the disc spreads quickly, in which case colours may evolve.
- (iii) By including a starburst extinction model, allowing the disc outer radius to float, and using the best-fit M_{\bullet} , a_{\bullet} , disc inclination, and mass accretion rates from our slim disc modeling of ASASSN-14li’s X-ray spectra, we successfully fit all four optical/UV light curves at $t > 350$ days (see Figure 2). This further substantiates the finding of (van Velzen, et al. 2019) that, contrary to simple time-dependent α -disc models (Shen & Magtzer 2014), most TDE discs remain both thermally and viscously stable during periods of radiation-dominated, sub-Eddington accretion.
- (iv) The application of the starburst galaxy dust extinction model provides the best and only good fit; the reduced χ^2 is about 1.6 for 43 degrees of freedom and the fitted disc radius is consistent with our prior X-ray spectral fits. This preferred extinction model is consistent with the fact that ASASSN-14li occurred in a post-starburst galaxy.
- (v) At late times, the fitted disc outer radius is about $2R_t$ and, at the 1σ CL, is consistent with a constant value. This is significantly less viscous spreading than would be expected in simple models. One relatively straightforward interpretation is that the ASASSN-14li inner disc lost large amounts of angular momentum, either due to preferential ejection directions during the circularization process (Bonnerot & Lu 2020) or in a magnetized wind (Blandford & Payne 1982).
- (vi) If ASASSN-14li’s early optical/UV emission is powered by a shock arising from intersecting debris streams, the mass of the disrupted star is $M_{\star} > 1.4M_{\odot}$ for $M_{\bullet} = 10^{6.5}M_{\odot}$, the low end of the ASASSN-14li black hole mass range ($10^{6.5-7.1}M_{\odot}$; 1σ CL; W20). For $M_{\bullet} > 10^{6.75}M_{\odot}$, the lower limit on progenitor mass becomes much more restrictive: $M_{\star} > 10M_{\odot}$. Standard stellar initial mass functions produce relatively few stars at this high mass, and even those stars should no longer exist in ASASSN-14li’s host galaxy, whose starburst ended ~ 400 Myr ago (French et al 2017). Thus, while shock power passes the self-consistency checks we pose in §5.1, it can only do so in a subset of the $\{M_{\bullet}, a_{\bullet}\}$ region that is allowed by the X-ray data.
- (vii) It is also possible that ASASSN-14li’s early optical/UV emission is generated through the reprocessing of X-ray emission from the inner disc. We checked whether this reprocessing can be achieved for ASASSN-14li with a reasonable mass budget, and found that the gas mass required to explain the optical/UV luminosity can be lower than $\sim 0.5M_{\odot}$, regardless of whether the reprocessing layer is static or outflowing in a wind. Because this mass budget is consistent with a reasonable progenitor star mass ($\sim 1M_{\odot}$ or less), the reprocessing

model cannot be excluded as an explanation of the early optical/UV emission. This result differs from some past work (Matsumoto & Piran 2021) in its consideration of a low covering fraction for wind reprocessing and of a quasi-static reprocessing layer; both of these options reduce the required mass relative to a spherical outflow.

Almost a decade after detection, ASASSN-14li remains a key laboratory for TDE physics. By fitting its late-time optical/UV light curve with a sequence of slim disc models, we have further confirmed previous observational conclusions that late-time TDE optical/UV emission is dominated by a bare, relatively compact, thermally stable accretion disc (van Velzen, et al. 2019). Somewhat surprisingly, this disc appears to have undergone little to no viscous spreading, which carries interesting implications for TDE disc physics.

We have shown that the combination of early-time X-ray and optical/UV datasets allows for novel consistency tests on different hypotheses concerning a central question in TDE physics: what is the geometry and power source of the early-time optical/UV photosphere? While in this case our consistency checks failed to falsify either the shock or reprocessing paradigms, they carried interesting implications for both, and may prove more decisive in future events. Specifically, X-ray bright TDEs with low optical/UV luminosities may struggle to self-consistently satisfy the shock paradigm, while (as already explored in (Matsumoto & Piran 2021)), the most optically bright TDEs run into self-consistency problems when described by the reprocessing picture.

While the near future carries the exciting prospect of hundreds if not thousands of TDE detections by ongoing and upcoming time-domain surveys, the scarcity of followup resources means that most of these events will lack the high-quality, multiwavelength coverage of past benchmark TDEs like ASASSN-14li. The unexpected persistence of late-time, slowly evolving disc emission shows that the “first generation” of TDEs may continue to yield scientific returns (and further surprises) long after they have become a minority of all TDEs.

ACKNOWLEDGEMENTS

We thank the referee for the helpful comments. SW thanks the Department of Astrophysics/IMAPP at Radboud University and the Department of Astronomy/Steward Observatory at the University of Arizona for post-doctoral support. SW also thanks Dongdong Shi for his useful discussion on host extinction models. NCS received financial support from the Israel Science Foundation (Individual Research Grant 2565/19) and the United States-Israel Binational Science Foundation (Grant No. 2019772). AIZ acknowledges support from NASA ADAP grant #80NSSC21K0988. She also thanks the hospitality of the Columbia Astrophysics Laboratory at Columbia University, where some of this work was completed. Our calculations were carried out at UA on the El Gato and Ocelote supercomputers, which are supported by the National Science Foundation under Grant No. 1228509.

DATA AVAILABILITY

The data underlying this article will be shared on reasonable request to the corresponding author.

REFERENCES

- Abramowicz, M. A., Czerny, B., Lasota, J. P., et al. 1988, *ApJ*, 332, 646. doi: [10.1086/166683](https://doi.org/10.1086/166683)
- Akaike, H., 1974, *IEEE Transactions on Automatic Control*, 19, 716, <https://ui.adsabs.harvard.edu/abs/1974ITAC...19..716A>
- Arcavi, I., Gal-Yam, A., Sullivan, M., et al., 2014, *ApJ*, 793, 1, doi: [10.1088/0004-637x/793/1/38](https://doi.org/10.1088/0004-637x/793/1/38)
- Arnaud K. A., 1996, in *Astronomical Society of the Pacific Conference Series*, Vol. 101, *Astronomical Data Analysis Software and Systems V*, Jacoby G. H., Barnes J., eds., p. 17.
- Bade, N., Komossa, S., & Dahlem, M., 1996, *A&A*, 309, L35
- Blandford, R. D. & Payne, D. G., 1982, *MNRAS*, 199, 883-903, doi: [10.1093/mnras/199.4.883](https://doi.org/10.1093/mnras/199.4.883)
- Bonnerot, C. & Lu, W., 2020, *MNRAS*, 495, 1374. doi: [10.1093/mnras/staa1246](https://doi.org/10.1093/mnras/staa1246)
- Brown, J. S., Holoien, T. W. -S., Auchettl, K. et al. 2017, *MNRAS*, 466, 4, doi: [10.1093/mnras/stx033](https://doi.org/10.1093/mnras/stx033)
- Calzetti, D., 1997, *AJ*, 113, 162, doi: [10.1086/118242](https://doi.org/10.1086/118242)
- Calzetti, D., Armus, L., Bohlin, R. C., et al., 2000, *ApJ*, 533, 682, doi: [10.1086/308692](https://doi.org/10.1086/308692)
- Cannizzo, J. K., Lee, H. M. & Goodman, J., 1990, *ApJ*, 351, 38, doi: [10.1086/168442](https://doi.org/10.1086/168442)
- Cardelli, J. A., Clayton, G. C. & Mathis, J. S., 1989, *ApJ*, 345, 245, doi: [10.1086/167900](https://doi.org/10.1086/167900)
- Coughlin, E. R., & Begelman, M. C., 2014, *ApJ*, 781, 2, doi: [10.1088/0004-637x/781/2/82](https://doi.org/10.1088/0004-637x/781/2/82)
- Dai, L., McKinney, J. C., & Miller, M. C. 2015, *ApJ*, 812, L39. doi: [10.1088/2041-8205/812/2/L39](https://doi.org/10.1088/2041-8205/812/2/L39)
- Dai, L., McKinney, J. C., Roth, N., Ramirez-Ruiz, E., & Miller, M. C. 2018, *ApJ*, 859, L20. doi: [10.3847/2041-8213/aab429](https://doi.org/10.3847/2041-8213/aab429)
- French, K. D., Arcavi, I., & Zabludoff, A., 2017, *ApJ*, 835, 2, doi: [10.3847/1538-4357/835/2/176](https://doi.org/10.3847/1538-4357/835/2/176)
- Ferrarese, L. & Ford, H., 2005, *ApJ*, 116, 3, doi: [10.1007/s11214-005-3947-6](https://doi.org/10.1007/s11214-005-3947-6)
- Ferreira, J. & Pelletier, G., 1995, *A&A*, 295, 807, <https://ui.adsabs.harvard.edu/abs/1995A&A...295..807F>
- Gehrels, N., Chincarini, G., Giommi, P. et al. 2004, *ApJ*, 611, 2, doi: [10.1086/422091](https://doi.org/10.1086/422091)
- Gezari, S., Martin, D. C., Milliard, B. et al. 2006, *ApJ*, 653, 1, doi: [10.1086/509918](https://doi.org/10.1086/509918)
- Gezari, S., Basa, S., Martin, D. C. et al. 2008, *ApJ*, 676, 2, doi: [10.1086/529008](https://doi.org/10.1086/529008)
- Gezari, S., Chornock, R., Rest, A. Et al. 2012, *Nature*, 485, 7397, 217, doi: [10.1038/nature10990](https://doi.org/10.1038/nature10990)
- Goodwin, A. J., van Velzen, S., Miller-Jones, J. C. A., et al. 2022, *MNRAS*, 511, 4, 5382, doi: [10.1093/mnras/stac333](https://doi.org/10.1093/mnras/stac333)
- Gordon, K. D., Clayton, G. C., Misselt, K. A. Et al., 2003, *ApJ*, 594, 1, doi: [10.1086/376774](https://doi.org/10.1086/376774)
- Greiner, J., Schwarz, R., Zharikov, S. & Orio, M., 2000, *A&A*, 362, L25, doi: [10.48550/arXiv.astro-ph/0009430](https://doi.org/10.48550/arXiv.astro-ph/0009430)
- Guillochon, J., & Ramirez-Ruiz, E., 2013, *ApJ*, 767, 1. doi: [10.1088/0004-637x/767/1/25](https://doi.org/10.1088/0004-637x/767/1/25)
- Guillochon, J., Manukian, H., & Ramirez-Ruiz, E., 2014, *ApJ*, 783, 23. doi: [10.1088/0004-637x/783/1/23](https://doi.org/10.1088/0004-637x/783/1/23)
- Guillochon, J. & Ramirez-Ruiz, E. 2015, *ApJ*, 809, 166. doi: [10.1088/0004-637x/809/2/166](https://doi.org/10.1088/0004-637x/809/2/166)
- Hayasaki, K., Stone, N., & Loeb, A., 2016, *MNRAS*, 461, 3760. doi: [10.1093/mnras/stw1387](https://doi.org/10.1093/mnras/stw1387)
- Hills, J. G., 1975, *Nature*, 254, 295. doi: [10.1038/254295a0](https://doi.org/10.1038/254295a0)
- Holoien, T. W.-S., Kochanek, C. S., Prieto, J. L., et al., 2016, *MNRAS*, 455, 2918. doi: [10.1093/mnras/stv2486](https://doi.org/10.1093/mnras/stv2486)
- Iglesias, C. A. & Rogers, F. J. 1996, *ApJ*, 464, 943, doi: [10.1086/177381](https://doi.org/10.1086/177381)
- James Conder, 2020, *MATLAB Central File Exchange*, <https://www.mathworks.com/matlabcentral/fileexchange/41775-f-test>,
- Jose, J., Guo, Z., Long, F. Et al., 2014, *The Astronomer's Telegram*, 6777, 1, <https://ui.adsabs.harvard.edu/abs/2014ATel.6777...1J>
- Kippenhahn, R. & Weigert, A., 1990, <https://ui.adsabs.harvard.edu/abs/1990MNRAS...190...100K>

[edu/abs/1990sse...book....K](https://ui.adsabs.harvard.edu/abs/1990sse...book....K)
 Kochanek C. S., 2016, MNRAS, 458, 127
 Komossa, S., Halpern, J., Schartel, N. Et al., 2004, ApJ, 603, 1, doi: [10.1086/382046](https://doi.org/10.1086/382046)
 Kormendy, J., & Ho, L. C., 2013, ARA&A, 51, 1, doi: [10.1146/annurev-astro-082708-101811](https://doi.org/10.1146/annurev-astro-082708-101811)
 STScI Development Team, 2013, strophysics Source Code Library, record ascl:1303.023, <https://ui.adsabs.harvard.edu/abs/2013ascl.soft03023S>
 Li, Z., French, K. D., Zabludoff, A. I. & Ho, L. C., 2019, ApJ, 879, 2, doi: [10.3847/1538-4357/ab1f68](https://doi.org/10.3847/1538-4357/ab1f68)
 Lightman, A. P. & Eardley, D. M., 1974, ApJ, 187, L1, doi: [10.1086/181377](https://doi.org/10.1086/181377)
 Lodato, G. & Rossi, E. M. 2011, MNRAS, 410, 359. doi: [10.1111/j.1365-2966.2010.17448.x](https://doi.org/10.1111/j.1365-2966.2010.17448.x)
 Loeb, A. & Ulmer, A. 1997, ApJ, 489, 573. doi: [10.1086/304814](https://doi.org/10.1086/304814)
 Lu, W., & Bonnerot, C. 2020, MNRAS, 492, 686. doi: [10.1093/mnras/stz3405](https://doi.org/10.1093/mnras/stz3405)
 Matsumoto, T. & Piran, T. 2021, MNRAS, 502, 3385. doi: [10.1093/mnras/stab240](https://doi.org/10.1093/mnras/stab240)
 McConnell, N. J. & Ma, C., 2013, ApJ, 764, 2, doi: [10.1088/0004-637X/764/2/184](https://doi.org/10.1088/0004-637X/764/2/184)
 Merritt, D., Alexander, T., Mikkola, S. & Will, C. M., 2010, Phys. Rev. D, 81, 6, doi: [10.1103/PhysRevD.81.062002](https://doi.org/10.1103/PhysRevD.81.062002)
 Metzger, B. D. & Stone, N. C. 2016, MNRAS, 461, 948. doi: [10.1093/mnras/stw1394](https://doi.org/10.1093/mnras/stw1394)
 Mockler, B., Guillochon, J., & Ramirez-Ruiz, E. 2019, ApJ, 872, 151. doi: [10.3847/1538-4357/ab010f](https://doi.org/10.3847/1538-4357/ab010f)
 Mockler, B., Twum, A. A., Auchettl, K. et al., 2022, ApJ, 924, 2, doi: [10.3847/1538-4357/ac35d5](https://doi.org/10.3847/1538-4357/ac35d5)
 Mummery, A. & Balbus, S. A., 2020, MNRAS, 492, 4, 5655-5674, doi: [10.1093/mnras/staa192](https://doi.org/10.1093/mnras/staa192)
 Roth, N., Kasen, D., Guillochon, J., et al. 2016, ApJ, 827, 3. doi: [10.3847/0004-637X/827/1/3](https://doi.org/10.3847/0004-637X/827/1/3)
 Psaltis, D., & Johannsen, T. 2012, ApJ, 745, 1. doi: [10.1088/0004-637X/745/1/1](https://doi.org/10.1088/0004-637X/745/1/1)
 Piran, T., Svirski, G., Krolik, J., et al. 2015, ApJ, 806, 164. doi: [10.1088/0004-637X/806/2/164](https://doi.org/10.1088/0004-637X/806/2/164)
 Piro, A. L. & Lu, W., 2020, ApJ, 894, 2. doi: [10.3847/1538-4357/ab83f6](https://doi.org/10.3847/1538-4357/ab83f6)
 Press, W. H., Teukolsky, S. A., Vetterling, W. T. & Flannery, B. P., 2002, <https://ui.adsabs.harvard.edu/abs/2002nrca.book....P>
 Prieto, J. L., Krühler, T., Anderson, J. P. et al. 2016, ApJ, 830, 2, L32, doi: [10.3847/2041-8205/830/2/L32](https://doi.org/10.3847/2041-8205/830/2/L32)
 Rees, M. J. 1988, Nature, 333, 523. doi: [10.1038/333523a0](https://doi.org/10.1038/333523a0)
 Roming, P. W. A., Kennedy, T. E., Mason, K. O. Et al., 2005 Space Sci. Rev., 120, 3-4, 95-142, doi: [10.1007/s11214-005-5095-4](https://doi.org/10.1007/s11214-005-5095-4)
 Roth, N., Kasen, D., Guillochon, J., et al. 2016, ApJ, 827, 3. doi: [10.3847/0004-637X/827/1/3](https://doi.org/10.3847/0004-637X/827/1/3)
 Roth, N. & Kasen, D. 2018, ApJ, 855, 54. doi: [10.3847/1538-4357/aaaec6](https://doi.org/10.3847/1538-4357/aaaec6)
 Roth, N., Rossi, E. M., Krolik, J. Et al. 2020, Space Sci. Rev., 216, 7, 114, doi: [10.1007/s11214-020-00735-1](https://doi.org/10.1007/s11214-020-00735-1)
 Rybicki, G. B., Lightman, A. P., 1979, <https://ui.adsabs.harvard.edu/abs/1979rpa...book....R>
 Jonker, P. G., Stone, N. C., Generozov, A., et al. 2020, ApJ, 889, 166. doi: [10.3847/1538-4357/ab659c](https://doi.org/10.3847/1538-4357/ab659c)
 Ryu, T., Krolik, J., Piran, T., et al. 2020, ApJ, 904, 98. doi: [10.3847/1538-4357/abb3cf](https://doi.org/10.3847/1538-4357/abb3cf)
 Saxton, R., Komossa, S., Auchettl, K. & Jonker, P. G., 2021, Space Science Reviews, 217, 1, 18, doi: [10.1007/s11214-020-00759-7](https://doi.org/10.1007/s11214-020-00759-7)
 Saxton, R. D., Read, A. M., Komossa, S. et al. 2017, A&A, 598, A29, doi: [10.1051/0004-6361/201629015](https://doi.org/10.1051/0004-6361/201629015)
 Scepi, N., Lesur, G., Dubus, G. & Flock, M., 2018, A&A, 620, A49, doi: [10.1051/0004-6361/201833921](https://doi.org/10.1051/0004-6361/201833921)
 Sfaradi, L., Rhodes, L., Williams, D., Bright, J. Et al., 2022, GRB Coordinates Network, <https://ui.adsabs.harvard.edu/abs/2022GCN.31667....1S>
 Shen, R. -F., Barniol Duran, R., Nakar, E. & Piran, T., 2015, MNRAS, 447, L60-L64, doi: [10.1093/mnras/lu183](https://doi.org/10.1093/mnras/lu183)

Table A1. Best-fit results for ASASSN-14li, with $M_{\bullet} = 10^7 M_{\odot}$ and $a_{\bullet} = 0.998$. In our simultaneous fitting, the M_{\bullet} and a_{\bullet} are held fixed, inclination is required to be the same for all epochs, and other parameters float. The total χ^2_{dof} is 4367.49/3895 = 1.12. The power-law parameters of epoch 6 are: $\Gamma = 1.6 \pm 0.7$ and $A_{\text{pl}} = 8.1 \pm 2.7 \times 10^{-6}$ photons $\text{s}^{-1} \text{cm}^{-2} \text{keV}^{-1}$.

Epoch	N_H [10^{20}cm^{-2}]	θ [$^{\circ}$]	\dot{m} [Edd]	$\chi^2/d.o.f$
1	5.4 ± 0.3	76 ± 3	1.09 ± 0.05	630.1/563
2	5.1 ± 0.2	...	1.03 ± 0.04	2322.33/2057
3	5.2 ± 0.3	...	1.06 ± 0.05	591.18/521
4	5.4 ± 0.4	...	0.44 ± 0.01	178.93/155
5	4.1 ± 0.3	...	0.35 ± 0.01	601.6/572
6	4.4 ± 0.3	...	0.335 ± 0.005	7.02/8
7	4.1 ± 0.4	...	0.227 ± 0.004	15.96/5
8	5.1 ± 0.5	...	0.206 ± 0.006	11.1/4
9	2.6 ± 0.8	...	0.150 ± 0.006	5.09/3
10	3.5 ± 0.8	...	0.130 ± 0.005	4.27/7

Shen, R. & Matzner, C. D., 2014, ApJ, 784, 2, doi: [10.1088/0004-637X/784/2/87](https://doi.org/10.1088/0004-637X/784/2/87)
 Shiokawa, H., Krolik, J. H., Cheng, R. M., et al. 2015, ApJ, 804, 85. doi: [10.1088/0004-637X/804/2/85](https://doi.org/10.1088/0004-637X/804/2/85)
 Steinberg, E. & Stone, N. C., 2022, arXiv: [2206.10641](https://arxiv.org/abs/2206.10641)
 Stone, N., Sari, R., & Loeb, A. 2013, MNRAS, 435, 1809. doi: [10.1093/mnras/stt1270](https://doi.org/10.1093/mnras/stt1270)
 Tout, C. A., Pols, O. R., Eggleton, P. P., & Han, Z., 1996 MNRAS, 281, 1, doi: [10.1093/mnras/281.1.257](https://doi.org/10.1093/mnras/281.1.257),
 Ulmer, A. 1999, ApJ, 514, 180. doi: [10.1086/306909](https://doi.org/10.1086/306909)
 van Velzen, S., Farrar, G. R., Gezari, S. Et al. 2011, ApJ, 741, 2, doi: [10.1088/0004-637x/741/2/73](https://doi.org/10.1088/0004-637x/741/2/73)
 van Velzen S., Stone N. C., Metzger B. D., Gezari S., Brown T. M., Fruchter A. S., 2019, ApJ, 878, 82. doi: [10.3847/1538-4357/ab1844](https://doi.org/10.3847/1538-4357/ab1844).
 van Velzen, S., Gezari, S., Hammerstein, E., et al. 2021, ApJ, 908, 4. doi: [10.3847/1538-4357/abc258](https://doi.org/10.3847/1538-4357/abc258)
 Wang, Y., Jiang, N., Wang, T. Et al., 2022, ApJ, 930, 1, L4, doi: [10.3847/2041-8213/ac6670](https://doi.org/10.3847/2041-8213/ac6670)
 Wen, S., Jonker, P. G., Stone, N. C., Zabludoff, A. I., Psaltis, D., 2020, ApJ, 897, 1. doi: [10.3847/1538-4357/ab9817](https://doi.org/10.3847/1538-4357/ab9817)
 Wen, S., Jonker, P. G., Stone, N. C., Zabludoff, A. I., 2021, ApJ, 918, 46. doi: [10.3847/1538-4357/ac00b5](https://doi.org/10.3847/1538-4357/ac00b5)
 Wen, S., Jonker, P. G., Stone, N. C., Zabludoff, A. I., & Zheng C., 2022, ApJ, 933, 1, 31, doi: [10.3847/1538-4357/ac70c5](https://doi.org/10.3847/1538-4357/ac70c5)
 Wevers, T., Pasham, D. R., van Velzen, S., Leloudas, G. et al. 2019, MNRAS, 488, 4, 4816-4830, doi: [10.1093/mnras/stz1976](https://doi.org/10.1093/mnras/stz1976),
 Waters, T. & Proga, D., 2018, MNRAS, 481, 2, 2628-2645, doi: [10.1093/mnras/sty2398](https://doi.org/10.1093/mnras/sty2398),
 Yang, C., Wang, T., Ferland, G. J. et al., 2017, ApJ, 846, 2, doi: [10.3847/1538-4357/aa8598](https://doi.org/10.3847/1538-4357/aa8598)

APPENDIX A: FITTING THE X-RAY SPECTRA WITH A SLIM DISC MODEL

We simultaneously refit the 10 epochs of X-ray spectra with the slim disc model of W21. The high-level fit assumptions are the same as in W20, i.e. all epochs have the same M_{\bullet} , a_{\bullet} and θ , but different absorption parameters N_H and \dot{m} .

Figure A1 shows the best fit to the 10 epochs of spectra. As shown in the figure, our model fits the spectra well, with the total reduced χ^2 being 1.12. The fitting parameters are listed in Table A1. The total χ^2 is about 1 smaller than that of 4368.42 in W20. The fitted N_H and θ are consistent with those in W20 at the 1σ CL. However, the fitted \dot{m} here are about 20% higher than those in W20 (note that \dot{m} presented here are not corrected for radiative efficiency). The slim disc model of W21 employed here differs from the earlier model in

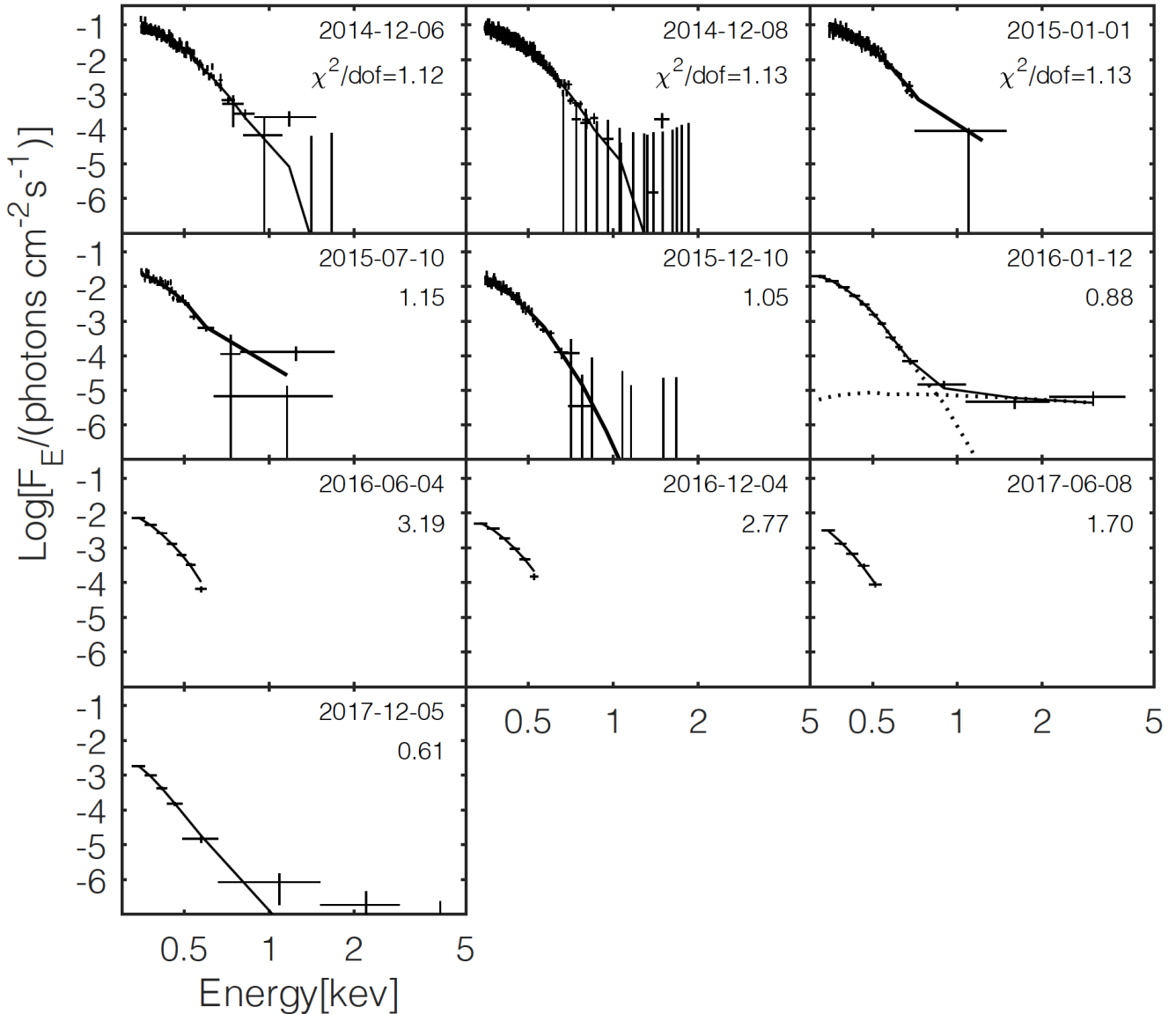


Figure A1. Simultaneous slim disk fits to XMM-*Newton* spectra of ASASSN-14li. The first five spectra are obtained using the two RGS detectors (we only plot RGS1), which provide data over the energy range 0.35–1.9 keV. The last five spectra are obtained using the pn detector, which is sensitive over 0.3–10 keV. All spectra are background-subtracted, and the data are binned so that there are at least 30 counts per bin. Each panel shows the best-fit model as a solid black line. In nine of the epochs, only the quasi-thermal disk model is needed to fit observations. In Epoch 6, however, we need an additional power-law component to fit the hard emission (horizontal dotted line). The fitting results are in Table A1.

W20 by including the effect of angular momentum loss by radiation. This effect will make the disc cooler, resulting in a higher fitted \dot{m} . However, both the W20 and W21 models produce similar constraints on M_\bullet and a_\bullet .

In order to constrain the decay of \dot{m} for each pair of M_\bullet and a_\bullet that lie within the 1σ contour of Fig. 6 of W20, we calculate the best-fit and 1σ error bars on the \dot{m} ¹⁵. We then fit the \dot{m} with a power law function $\dot{m}_t = A(t + 150)^{-n}$, where A and n are free parameters to be fitted. Figure A2 shows the power law fitting result for 4 pairs of

M_\bullet and a_\bullet . We can see that the decay in the accretion rate can be well fit by a power law function, especially for the late time epochs.

APPENDIX B: DISC SPREADING

In this Appendix, we derive a toy model for the time evolution of a viscously spreading disc, to derive approximate expectations for the evolution of its outer radius R_{out} . We assume the disc possesses a surface mass density profile $\Sigma(R) = \Sigma_{\text{out}}(R/R_{\text{out}})^{-\Gamma}$ for all radii $R_{\text{ISCO}} \leq R \leq R_{\text{out}}$, and has no mass elsewhere. We assume that the disc begins with an initial mass $M_\star/2$, or in other words the entire bound mass of the disrupted star. This approach, similar to

¹⁵ Here we use slim disc model `s1imd` (Wen et al. 2022) to do the fitting. We note that `s1imd` is the tabulated version of W21.

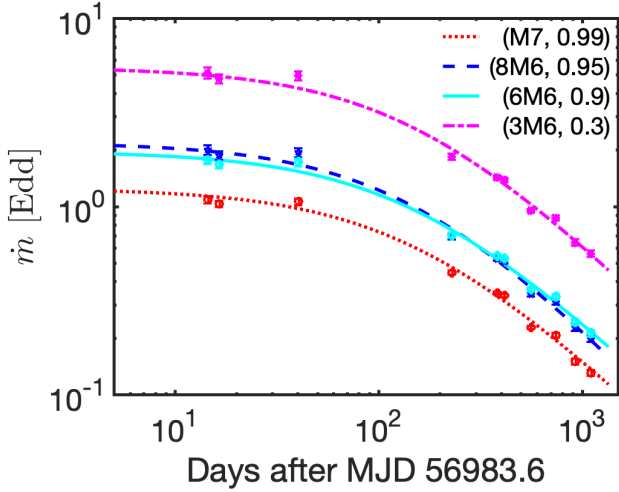


Figure A2. Dimensionless accretion rates \dot{m} for four $\{M_{\bullet}, a_{\bullet}\}$ pairs obtained from X-ray spectral fitting, along with the corresponding best fit power-law $\dot{m}(t)$ functions. The equations are $\dot{m}_t = 231(t + 150)^{-1.04 \pm 0.02}$, $\dot{m}_t = 658(t + 150)^{-1.14 \pm 0.03}$, $\dot{m}_t = 361(t + 150)^{-1.04 \pm 0.02}$, and $\dot{m}_t = 1227(t + 150)^{-1.08 \pm 0.02}$, from top to the bottom of the legend, respectively.

that in (van Velzen, et al. 2019) and (Mummery & Balbus 2020), will be quite inaccurate at early times, but should be reasonably accurate at late times when $t_{\text{visc}} \gg t_{\text{fall}}$. The instantaneous disc mass $M_d = M_{\star}/2 - \Delta M$, where ΔM is the total mass accreted so far. The instantaneous disc angular momentum $L_d = (M_d + \Delta M)J_{\text{circ}} - \Delta L$, where $J_{\text{circ}} = \sqrt{2GM_{\bullet}R_{\text{circ}}}$ is the specific angular momentum of the disrupted star and $\Delta L = J_{\text{ISCO}}\Delta M$ is the angular momentum lost into the event horizon through accretion. As this is just a toy model, we crudely assume that $J_{\text{ISCO}} = \sqrt{GM_{\bullet}R_{\text{ISCO}}}$, and that $R_{\text{ISCO}} = 6R_g$.

By integrating over the disc size, we find that $\Sigma_{\text{out}} \approx (2 - \Gamma)M_d/(2\pi R_{\text{out}}^2)$ so long as $\Gamma < 2$. Likewise, we find that $L_d \approx 2\pi(5/2 - \Gamma)^{-1}\Sigma_{\text{out}}\sqrt{GM_{\bullet}R_{\text{out}}^{5/2}}$ so long as $\Gamma < 5/2$. In both cases the approximate equalities come from assuming that $R_{\text{out}} \gg R_{\text{ISCO}}$, and the assumptions on Γ are likely valid (for example, in the radiation-dominated regime of a Shakura-Sunyaev disc, $\Gamma = -3/2$).

We now combine these approximate equalities with our earlier statements of mass and angular momentum conservation to solve for the expanding outer edge of the spreading disc:

$$R_{\text{out}} = \left(\frac{5/2 - \Gamma}{2 - \Gamma} \right)^2 \left(\frac{M_{\star}\sqrt{R_{\text{circ}}/2} - \Delta M\sqrt{R_{\text{ISCO}}}}{M_{\star}/2 - \Delta M} \right)^2. \quad (\text{B1})$$

As an example, consider $R_{\text{ISCO}} = 6R_g$ and $R_{\text{circ}} = 100R_g$. This equation then implies that if the disc has lost 80% of its initial mass ($\Delta M = 0.8M_{\star}/2$), then R_{out} should expand by a factor ≈ 19 . As we see in Fig. 3, no evidence for significant disc spreading is seen. There are a few plausible explanations for this. First, it is possible that very little of the disc mass has actually accreted onto the MBH. In the above example, if $\Delta M = 0.2M_{\star}/2$, then R_{out} will only grow by a factor ≈ 1.4 , which is marginally consistent with Fig. 3.

A second possibility is that our assumption that $\Delta L = J_{\text{ISCO}}\Delta M$ is incorrect, and that there is a more important additional source of angular momentum loss. For example, if large amounts of angular momentum are lost in a magnetized wind (Waters & Proga 2018) (as is seen in MHD simulations of super-Eddington accretion discs), this may dominate ΔL and limit the disc's ability to spread. More speculatively, the early time shocks between the disc and returning debris

streams may preferentially eject high-angular momentum material from the system, starving the disc of its angular momentum budget.

A third possibility is that $R_{\text{circ}} \approx R_{\text{ISCO}}$, or in other words that this was a rare, high- β TDE. However, a significant degree of fine-tuning is needed to eliminate observable changes in R_{out} through this explanation.